

PHYSICS OF OUR DAYS

PACS numbers: **42.55. – f**, 42.65.Jx, 42.65.Rc

Nonlinear compression of high-power laser pulses: compression after compressor approach

E A Khazanov, S Yu Mironov, G Mourou

DOI: https://doi.org/10.3367/UFNe.2019.05.038564

Contents

1. Introduction **1096**
1.1 Limitations on the peak power of modern lasers; 1.2 Concept of nonlinear laser-pulse compression; 1.3 History of nonlinear compression of laser pulses; 1.4 Limitations on the nonlinear compression of pulses higher than 1 TW in power

2. Theoretical foundations of phase self-modulation and compression **1100**
2.1 Basic equation, effects, and parameters of the problem; 2.2 Compression-after-compressor approach (CafCA) in a one-dimensional quasistationary model; 2.3 Special features for pulses several hundred femtoseconds in duration; 2.4 Special features for pulses shorter than 15 fs

3. Compression nonuniformity over beam cross section **1106**
3.1 Large-scale self-focusing; 3.2 Nonuniform pulse shortening; 3.3 Nonlinear wavefront distortions

4. Small-scale self-focusing of ultrahigh-power laser beams **1109**
4.1 Theory of small-scale self-focusing; 4.2 Special feature of small-scale self-focusing in ultrahigh-power lasers: a large critical angle; 4.3 Suppression of small-scale self-focusing by beam self-filtering; 4.4 Suppression of small-scale self-focusing by nonlinear dispersion; 4.5 Application of traditional small-scale self-focusing suppression methods in ultrahigh-power lasers

5. Plastic: a new promising nonlinear material **1116**
5.1 Idea of using plastics; 5.2 Increasing the critical angle of small-scale self-focusing; 5.3 Two-stage compression; 5.4 Nonlinear element fragmentation

6. Compression after compressor approach (CafCA): status quo and prospects **1118**
6.1 Review of experiments with a pulse power of 0.2–250 TW; 6.2 Numerical CafCA simulations for petawatt pulses; 6.3 Future research avenues

7. Conclusions **1121**

References **1122**

Abstract. The peak power of present-day lasers is limited by the pulse energy that the diffraction gratings of an optical compressor can withstand. A promising method to overcome this limitation is reviewed: the pulse power is increased by shortening its duration rather than increasing the pulse energy, the pulse being shortened after passing a compressor (Compression after Compressor Approach (CafCA)). For this purpose, the pulse spectrum is broadened as a result of self-phase modulation, and the pulse is then compressed by dispersion mirrors. Application of this idea, known since the 1960s, to lasers whose power is over 1 TW has been restrained until recently by a number of physical problems. These problems and possible methods to solve them are discussed in detail. The experimental results obtained over the past few years demonstrate the efficiency of the technique (compression by a factor of 5) in the range up to 250 TW. CafCA features three undisputed merits: simplicity and low cost, negligible loss of pulse energy, and applicability to any high-power laser.

Keywords: ultrahigh power femtosecond lasers, phase self-modulation, nonlinear laser pulse compression, small-scale self-focusing

E A Khazanov [(1,*)], **S Yu Mironov** [(1,†)], **G Mourou** [(2,‡)]
[(1)] Institute of Applied Physics, Russian Academy of Sciences, ul. Ul'yanova 46, 603000 Nizhny Novgorod, Russian Federation
[(2)] International Center for Zetta-Exawatt Science and Technology, Route de Saclay, Palaiseau, F-91128, France
E-mail: [(*)] efimkhazanov@gmail.com, [(†)] sergey.mironov@mail.ru, [(‡)] gerard.mourou@polytechnique.edu

Received 12 May 2019
Uspekhi Fizicheskikh Nauk **189** (11) 1173 – 1200 (2019)
DOI: https://doi.org/10.3367/UFNr.2019.05.038564
Translated by E N Ragozin; edited by V L Derbov

1. Introduction

1.1 Limitations on the peak power of modern lasers

Since the development of the first laser by Theodore Maiman in 1960 [1], the pursuit of ultrahigh fields has been one of the main focuses in laser physics, i.e., the pursuit of record high intensity of focused electromagnetic radiation, which may be estimated by the formula

$$I_{\text{focus}} \approx \frac{P}{\lambda^2}\left(\frac{\Theta_{\text{beam}}}{\Theta_{\text{dif}}}\right)^2, \qquad (1)$$

where $P = W/\tau$ is the peak pulse power, W and τ are its energy and duration, λ is the wavelength, Θ_{beam} is the beam divergence, and Θ_{dif} is the diffraction-limited divergence. It

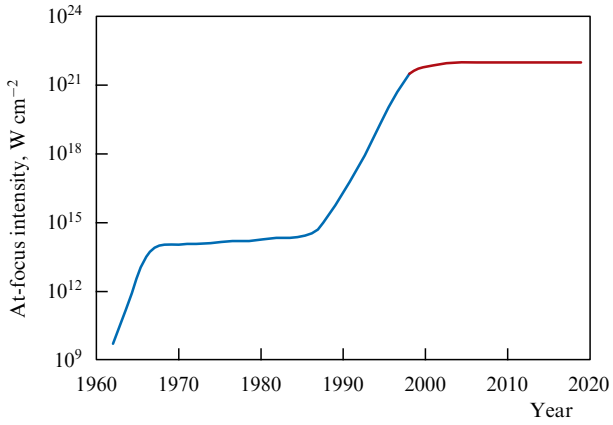

Figure 1. (Color online.) At-focus intensity of laser radiation. The dependence from 1960 to 1998 was borrowed from Ref. [2].

became immediately clear that lasers have no rivals among microwave radiation sources or among incoherent sources of light and shorter-wavelength radiation. Microwave sources rank far below because of significantly longer λ and τ. Incoherent sources, even for a shorter wavelength than the laser wavelength (ultraviolet (UV) and X-ray ranges), are at a disadvantage owing to a greater divergence Θ_{beam}, which is many orders higher than Θ_{dif}.

In just a few years after their advent, lasers revealed their significant advantages by reaching an intensity of 10^{14} W cm^{-2}. However, the radiation intensity hardly increased during the next 20 years [2] (Fig. 1). The reason for this 'plateau' lay with the fact that laser amplifiers had reached their limit related to the optical breakdown threshold of the medium. To state it in different terms, in an attempt to scale up the laser radiation, it damaged the amplifier itself. Therefore, the unresolvable contradiction was that, on the one hand, a pulse had to gain energy from the medium to be amplified, i.e., to propagate through the medium, but, on the other hand, the pulse itself damaged the medium. By way of analogy to a laser pulse, one may consider a worm which we want to fatten. For this purpose, we have an unlimited amount of food stored in a long tube. When crawling along the tube, the worm (the pulse) eats and increases in mass (energy). Evidently, nothing limits the growth of the worm's mass if the worm grows in length. However, the worm's diameter (the pulse power) may only grow up to the tube diameter. Further worm thickening is impossible inside the tube, but there is no food outside of the tube.

In 1985, Donna Strickland and Gerard Mourou proposed a way out [3]. First, a laser pulse is stretched in time (by 4–5 orders of magnitude) with a corresponding decrease in power. After that, the pulse is amplified to the limiting power and then compressed (Fig. 2a). As a result, the compressed pulse power exceeds the breakdown threshold of laser amplifiers by several orders of magnitude. Therefore, the implementation of the idea calls for three devices: (i) a stretcher, which stretches the pulse and lowers its intensity without a change in energy; (ii) an amplifier, which increases the energy and power of the pulse but does not change its duration; (iii) a compressor, which shortens the pulse and increases its power without increasing its energy.

A stretcher is a dispersive device, which delays different wavelengths by different time intervals. As a result, a short laser pulse in which all wavelengths are synchronous spreads in time: 'red' wavelengths are in advance and the 'blue' ones are behind, or vice versa, depending on the sign of dispersion. These pulses are referred to as chirped, and the proposed concept has received the name 'Chirped Pulse Amplification' (CPA). We emphasize that chirped (or frequency-modulated) pulses also occur in other realms of physics: from radar (where the term itself was borrowed from) to gravity waves — it was precisely the chirped pulse of gravity waves that was detected by the LIGO (Laser Interferometer Gravitational-wave Observatory) collaboration [4], which was awarded the Nobel Prize in Physics in 2017.

For CPA, it is fundamentally important that the energy of a pulse does not increase in its compression, i.e., use can be made of purely reflective optical elements — diffraction gratings. A negative-dispersion compressor based on diffraction gratings was invented and implemented back in 1968 by Edmund Treacy [5], who described the operation of this compressor in detail in Ref. [6]. Before 1985, the Treacy compressor was repeatedly used for precisely the compression of chirped pulses, but not for CPA. Efficient operation with short, i.e., broadband, pulses requires a stretcher that introduces positive dispersion, which is the same (in modulus) as in the Treacy compressor. Although the simple and convenient fiber stretcher employed in Ref. [3] introduces positive dispersion, it is a poor match for the Treacy

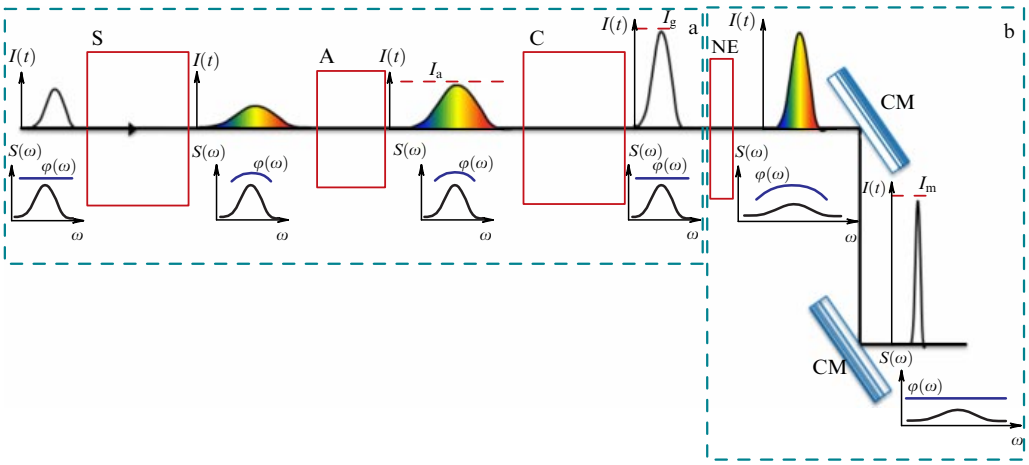

Figure 2. (Color online.) CPA (a) and CafCA (b) concepts. S — stretcher, A — laser amplifier, C — compressor, NE — nonlinear element, CM — chirped mirror; I_a , I_g, and I_m are the breakdown thresholds of amplifiers, diffraction gratings, and chirped mirrors.

compressor, since the shapes of the dispersion dependences of fibers and diffraction gratings are much different. A 'suitable' device comprising diffraction gratings and a lens telescope was proposed in Ref. [7] by Oscar Martinez, who employed it as a compressor for CPA in a wavelength region of 1.5 μm, where the dispersion of the fiber stretcher is negative. Five months later, in the same year of 1987, M Pessot et al. published a paper [8] in which the Martinez device was employed precisely as the stretcher in combination with the Treacy compressor. More recently, to eliminate the dispersion introduced by the lenses, the lens telescope in the Martinez stretcher was replaced by a mirror one, in accordance with Abe Offner's patent [9]. For a detailed review of different operational aspects of stretchers and compressors, the reader is referred, e.g., to Ref. [10]. At present, virtually all high-power lasers comprise three elements: (i) Offner's diffraction-grating stretcher with a positive dispersion; (ii) an amplifier; (iii) Treacy's diffraction-grating compressor with a negative dispersion.

The invention of CPA resulted in a sharp rise in laser power, which is clearly demonstrated by Fig. 1: in the late 1980s, the plateau was replaced by quick growth. By the early 2000s, the intensity became as high as 10^{22} W cm^{-2} [11, 12]. However, the intensity has hardly risen since then — the second plateau made its appearance. It is valid to say that humankind has made the most of the CPA concept. The reason was that by the early 2000s the power (and the intensity) had risen so much that it was limited not by the impossibility of amplifying laser pulses still further but by the impossibility of compressing them even more strongly. Diffraction gratings have a finite breakdown threshold, which limits the output CPA-laser intensity. In the near future, such gratings will permit making lasers with an output power of 10 PW and an intensity of 10^{23} W cm^{-2}. Therefore, the weak link in the stretcher–amplifier–compressor chain is the compressor.

What next? There are three ways to raise the laser power and intensity. The first is to make a mosaic (tiled) compressor [13–15]. Each grating of such a compressor consists of several diffraction gratings, which increases the beam aperture several-fold. This makes it possible to compress pulses of higher energy. The second is to make parallel phased CPA channels, each of which is equipped with its own compressor [16–19]. These two ways have several significant drawbacks: the existence of technical and technological problems, the necessity of increasing the pulse energy several-fold, as well as the large size and high cost of the laser. In this review, we will not discuss these two ways and will restrict ourselves to a discussion of the third way, which is by far simpler and cheaper: increasing the power by pulse shortening rather than by increasing the pulse energy.

1.2 Concept of nonlinear laser-pulse compression

The pulse duration at the CPA-laser output (after Treacy's compressor) is, as a rule, only slightly longer than the Fourier limit. So, to significantly shorten the pulse requires broadening its spectrum, i.e., stretching not the pulse length, as in CPA, but stretching its spectrum. For this purpose, a nonlinear element is needed to be used (Fig. 2b). The simplest and most suitable element is a plate with a cubic (Kerr-type) nonlinearity, whose refractive index n depends on the intensity I:

$$n = n_0 + n_2 I, \tag{2}$$

where n_0 is the linear refractive index and n_2 is the nonlinear refractive index determined by the cubic nonlinearity tensor $\chi^{(3)}$. As is clear from Eqn (2), in this case, the pulse propagates through a medium in which the refractive index varies in time, since $I = I(t)$. This gives rise to phase modulation (to be more precise, to self-modulation) and therefore to spectral pulse broadening. However, this is only a necessary condition for pulse shortening; required in addition is the phase synchronism of all frequencies of the spectrum. The pulse becomes chirped at the output of the nonlinear element. To state it in different terms, the nonlinear element introduces dispersion (the frequency dependence of the spectral phase), which must be compensated by adding the same (in modulus) dispersion of opposite sign, just as is done by a compressor in CPA. The magnitude of this dispersion is much smaller than that introduced by the Treacy compressor, and therefore advantage is taken of chirped mirrors. These mirrors cannot be employed in CPA instead of diffraction gratings, since they introduce only a small dispersion, but in return their breakdown threshold is higher than for gratings. Owing to this circumstance, the pulse power may exceed the breakdown threshold of the gratings (Fig. 2b).

This way of nonlinear compression of laser pulses has received the name Thin Film Compression (TFC) [20] or Compression after Compression Approach (CafCA) [21, 22]. In what follows, we use the latter name. CafCA offers three indisputable advantages. First, simplicity and cheapness: required are only a plane-parallel plate and one or several chirped mirrors, whose fabrication technology has been adequately developed [23–27] and which are extensively used in femtosecond lasers. Second, the possibility of application to practically any high-power laser, no laser alteration being required. Third, a high efficiency: the energy loss is under 1%, provided the nonlinear element is mounted at a Brewster angle.

The key parameter that defines the spectrum broadening as well as the pulse shortening and the increase in peak power is nonlinear phase incursion. As is easily seen from Eqn (2), the incursion is defined by the so-called decay integral, or the B-integral:

$$B = kLn_2 I. \tag{3}$$

Here, L is the length of the nonlinear element, $k = 2\pi/\lambda_0$, and λ_0 is the central vacuum wavelength of the radiation.

1.3 History of nonlinear compression of laser pulses

The idea of compressing laser pulses by way of phase modulation with the subsequent compensation of dispersion was proposed by J Giordmaine et al. [28] in 1968 by analogy with pulse compression in chirped radars [29, 30]. To realize phase modulation, the authors of Ref. [28] used an electro-optical crystal, to which they applied sinusoidal voltage. The laser pulse passed through the crystal at the instant of zero phase, i.e., the pulse frequency varied linearly in time. A four-fold broadening of the helium-neon laser spectrum was demonstrated. In Ref. [31], a 500-ps-long pulse was not only chirped with an electrooptical crystal, but was also compressed to 270 ps using a Gires–Tournois interferometer [32].

The key idea — to use cubic nonlinearity for self-phase modulation (SPM) — was proposed by Robert Fisher et al. in 1969 [33]. In Ref. [33], they provided a theoretical substantiation of the method and showed the promise of using liquid CS_2 as the nonlinear medium and the Kerr effect as the

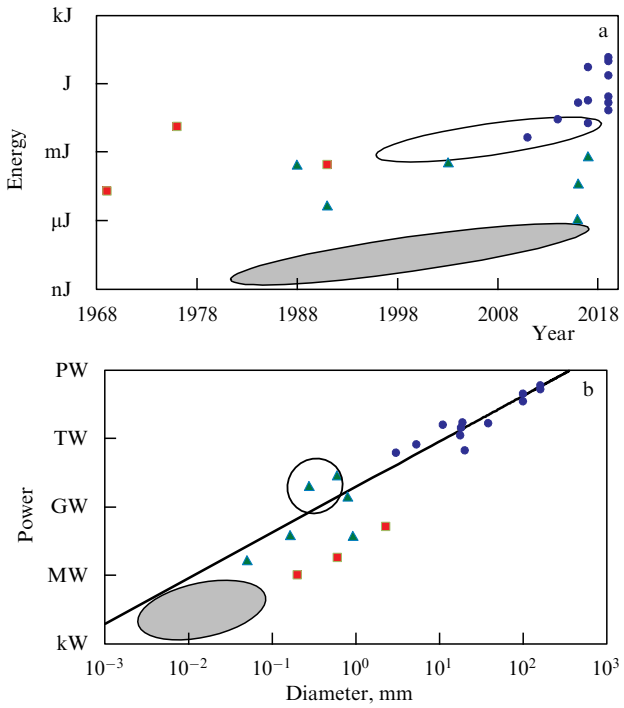

Figure 3. (Color online.) (a) Energy and (b) peak power of laser pulses in experiments with nonlinear compression: SPM was performed in a liquid (red squares [34–36]), in a fiber (shaded ellipse), in HCF (empty ellipse), in a volume with limited propagation (green triangles [66–71]), and in a volume with free propagation (blue circles [22, 76–85]). The straight line corresponds to an intensity of 1 TW cm^{-2}.

nonlinear effect. That same year, A Laubereau [34] realized this idea by compressing several-fold a 20-picosecond pulse with the use of CS_2-filled cells 14 cm in total length and a Treacy compressor. Laubereau's work [34] was the first experimental implementation of CafCA (Fig. 3a). More recently, this experiment was repeated at a significantly higher energy and with a stronger compression: from 96 ps to 6.9 ps in Ref. [35] and from 45 ps to 2 ps in Ref. [36], where use was made of a CS_2-filled capillary. A significant disadvantage of liquids is the long relaxation time of the Kerr nonlinearity (2 ps for CS_2), which limits the duration of compressed pulses to the picosecond range. This is supposedly why the idea was 'forgotten' and was rekindled in the 1980s in connection with the development of femtosecond dye lasers and fiber technology.

Fiber was first used for SPM in Ref. [37], in which pulses were compressed from 5.5 ps to 1.5 ps employing a 70-m-long single-mode fiber and a compressor in the form of a cell with sodium vapor, which introduced high dispersion owing to the transition at a frequency close to the laser frequency. In 1982, compression was first realized in the femtosecond range [38]. A 90-fs-long pulse several nJ in energy was focused into a 15-cm-long fiber, after which the Treacy compressor squeezed it to 30 fs. The 1980s saw a wealth of theoretical [39–41] and experimental [42–48] studies. In particular, demonstrated was a two-stage 65-fold pulse compression [43] and a compression to 6 fs [47], when a prism compressor was employed in addition to Treacy's compressor; use was made of a gradient fiber with a large mode diameter [48]. The input pulse energy amounted to several μJ and the power ranged up to the submegawatt level [44, 46]. Investigations in this area were continued and are now underway, but a further increase in energy is obviously limited by the very small diameter of the fiber.

The energy may be significantly increased (from several nJ to several mJ) if gas-filled hollow core fibers (HCFs) or capillaries are used instead of single-mode fibers, as proposed in Ref. [56] in 1996. The limitations on the pulse energy in HCFs are far less stringent owing to an increase in, first, beam diameter — from several micrometers to several hundred micrometers — and, second, breakdown (or ionization) threshold. Impressive results were obtained in the same pioneering work [56]: a 140-fs-long pulse was compressed to 10 fs after passing through a 70-cm-long HCF 140 μm in diameter filled with krypton at a pressure of 2 atm and a compressor consisting of a pair of prisms. The pulse energy lowered from 0.66 mJ to 0.22 mJ. At the same time, titanium-sapphire lasers [57] came into wide use, and several nonlinear compression experiments were performed using them (see, e.g., Refs [58–64]). Among these results, mention should be made of the production of a 3.8-fs-long pulse [58] and the use of an HCF with a pressure gradient [63], a capillary 0.42 mm in diameter [59], and a circularly polarized pulse [61]. The input pulse energy became as high as a few tens of mJ and the power reached the subterawatt level (see Fig. 3). It is significant that the energy transmittance of HCFs is usually less than 50%. However, this is abundantly compensated by pulse shortening, by approximately 10 times, and by a factor of 33 in Ref. [33]. At the same time, advancement to significantly higher energies and powers requires a corresponding increase in HCF diameter, which seems to be impossible.

An alternative (apart from HCFs) to single-mode fibers is a bulk solid nonlinear element, in which a laser beam propagates freely. In this case, the problem of limited beam aperture is removed in a natural way, but problems related to the spatial nonuniformity of the beam inevitably arise. First and foremost, this is the nonuniform incursion of the nonlinear phase, which is proportional to the intensity (2). This results in two effects: beam self-focusing and transversely nonuniform spectral broadening and, therefore, nonuniform beam compression. In particular, at the beam periphery, where the intensity is much lower than on the axis, the compression practically vanishes. In a single-mode fiber (and to a large extent in an HCF), the nonlinear phase is added to the entire beam as a whole and all spatial effects are simply missing. A comprehensive theoretical analysis of the above spatial effects was performed in Ref. [65], which showed that they impose significant limitations.

Several ways of solving the spatial nonuniformity problem were investigated. In 1988, it was suggested that the beam be stopped down immediately after its passage through the nonlinear element, thereby keeping only the paraxial beam domain. The authors of Ref. [66] experimentally studied the possibility of a trade-off between efficient pulse shortening (minimal aperture size) and minimal energy loss (maximum aperture size). The results suggested that quasi-uniform four-fold pulse compression may be obtained for an aperture stop transmission of no higher than 25–35%. In Ref. [67], the aperture stop was placed in the far-field zone rather than immediately after the nonlinear element. This also resulted in a 3.5-fold quasi-uniform pulse compression for a transmittance of only 35%. In Ref. [68], the beam was focused on the nonlinear element with a cylindrical lens in such a way so as to realize soliton-like propagation in the direction of the smaller size: diffraction was completely compensated by self-

focusing. However, in this experiment, the loss was even higher. In Ref. [69], efficient compression was realized when crystalline quartz was placed near or directly in the focal plane of a lens, but evidently this approach cannot be scaled up. In Ref. [70], the beam passed through seven nonlinear plates, which were spaced so that self-focusing in each of them was compensated by diffraction in the propagation to the next one. A similar 'multipass' idea with spherical mirrors was realized in Ref. [71]: 38 transits through the nonlinear medium. In both papers, it was possible to avoid significant loss and compress the pulse by about a factor of five at energies of 0.8 mJ and 0.05 mJ, respectively. However, the authors of Ref. [71] did not demonstrate the uniformity of compression and, most important, scaling so complicated a system up to at least joule levels seems to be hardly realizable. Therefore, despite endeavors to eliminate the adverse effect of spatial nonuniformity, attempts have failed to advance even to a power of 0.1 TW and reach the values mastered with the help of HCFs (see Fig. 3).

The feasibility of CafCA for lasers of significantly higher power with a quasi-uniform intensity distribution is discussed in Refs [72–76]. A several-fold spectral broadening of second-harmonic pulses for an energy of 4.7 mJ and a beam diameter of 3 mm was experimentally observed in Ref. [76]. Because of the absence of chirped mirrors for the second-harmonic wavelength (460 nm), pulse compression was not realized. A start was nevertheless made on the experimental investigation of nonlinear pulse compression in its modern form (see Fig. 3). A number of experimental results were obtained in recent years [22, 77–85], where CafCA was successfully realized at a power of 0.2–250 TW (indicated with circles in Fig. 3). The proposed and experimentally confirmed method for the suppression of small-scale self-focusing [86], which permits the multiplicity of compression to be significantly increased, became an important motivation for these investigations. Furthermore, theoretical investigations were performed [20, 79, 87], related to the petawatt and multipetawatt power level, and it is precisely the 1 TW–10 PW power range that our review is concerned with. Before setting forth our statement in detail, we discuss the physical mechanisms which impose significant limitations on CafCA at a high power.

1.4 Limitations on the nonlinear compression of pulses higher than 1 TW in power

As indicated above, the SPM of pulses 1 TW and above in power is possible only in free propagation in a solid. As shown in Refs [72, 88], stimulated Raman scattering does not limit the power pulse. There are three problems which impede to a greater or lesser extent the implementation of CafCA.

The first is the intensity nonuniformity mentioned above, which is responsible for the self-focusing of a beam as a whole, i.e., for large-scale self-focusing, phase aberrations and, most important, for nonuniform beam compression. A solution to the last-named problem — the use of a negative lens as the nonlinear element — was proposed in Ref. [89] and then realized experimentally in Refs [77, 78], which immediately transferred CafCA from the millijoule range to the range of several tens and hundreds of mJ. The parasitic effects related to the nonuniform distribution of beam intensity, as well as methods to suppress them, are minutely considered in Section 3.

Second, this is small-scale self-focusing (SSSF). Unlike the large-scale one, which arises from the nonuniformity of beam intensity, SSSF is present even in a plane wave, since it is caused by the Bespalov–Talanov instability [90]. The instability increment is due to the B-integral (3). For $B = 2-3$, the beam usually divides into filaments, which results in a significant impairment of beam quality [91], uncontrollable spectral broadening [92], and the breakdown of optical elements. At the same time, multiple pulse compression is impossible for $B < 2-3$ (for more details, see below). On the face of it, the task of significant CafCA-assisted power enhancement therefore seems to be unrealizable: the same effect (cubic nonlinearity) is simultaneously useful and parasitic, this being so for the same parameter value (B-integral). In view of this, until recently it was believed (see, e.g., Refs [72, 74, 88, 93]) that CafCA is possible only in the narrow range $2 < B < 3$, which permits expecting no more than a 2- to 2.5-fold compression (see Section 2). As demonstrated in Ref. [86], efficient suppression of SSSF for high-power femtosecond lasers is possible using beam self-filtering on propagation in free space. This permits a significant increase in the admissible values of the B-integral and, accordingly, in the multiplicity of compression. Section 4 is concerned with the features of SSSF in ultrahigh-power lasers and with methods to suppress it.

The third is a technological problem, which is most pronounced at a petawatt power level: the very high ratio between the diameter of a nonlinear element and its thickness. As the power becomes higher, the beam diameter increases and the nonlinear element becomes thinner. It is significant that the nonlinear element should not introduce significant linear wavefront distortions, which would impair the beam focusing. The production technology of traditional optical elements of glass and silica is under development, but a significant advancement in the solution to this problem was made possible by the idea in [20, 94] of employing polymer materials. Their production technology readily provides polymers with thicknesses of the order of 100 μm with a meter-sized aperture. Both the linear and nonlinear optical properties of polymer materials are now actively being studied, and the results are highly promising. In particular, a pulse 100 TW in power was compressed by a factor of 2.6 [80]. The special features of employing polymer materials for CafCA are considered in Section 5.

Section 2 is dedicated to the theoretical aspects of SPM and the determination of the key effects and the parameters responsible for them. In Sections 3–5, we expound on the three specified groups of problems and outline ways to solve them, which have made it possible to master the 1–250 TW range and have opened the way to petawatt and multipetawatt ranges. Section 6 reviews experimental results and avenues of future investigations.

2. Theoretical foundations of phase self-modulation and compression

The propagation of a pulse in media with Kerr nonlinearity is the concern of a wealth of papers. The first of them [33, 95–102] were published in the 1960s only a few years after the advent of the first laser. These investigations have continued since then (see, for instance, Refs [103–110] and references therein). As mentioned in Section 1.3, the SPM effect under discussion is at the heart of the techniques of spectral broadening in fibers [38, 39], gas-filled capillaries [56], and transparent solid dielectrics [65, 67]. The effects included in theoretical models depend on the pulse and medium para-

meters. Of importance are regimes occurring for a minimal modification of the laser pulse and medium parameters [20, 80], as well as regimes attended by plasma production and the generation of white light [103, 111, 112]. In Sections 2.1–2.4, we consider a mathematical model describing the propagation of high-intensity pulses in a medium with Kerr nonlinearity, the limits of its applicability, and the results obtained on its basis.

2.1 Basic equation, effects, and parameters of the problem

Under the slowly varying amplitude approximation, the propagation of laser pulses in a medium with Kerr nonlinearity is described by the generalized nonlinear Schrödinger equation [103, 105, 107, 113]:

$$\frac{\partial A}{\partial z}+\frac{1}{u}\frac{\partial A}{\partial t}+\frac{\mathrm{i}}{2k}\Delta_\perp A-\mathrm{i}\frac{k_2}{2}\frac{\partial^2 A}{\partial t^2}+\frac{3\pi\chi^{(3)}}{2n_0c}\times\left(\mathrm{i}\omega_0|A|^2A+2A\frac{\partial|A|^2}{\partial t}+2|A|^2\frac{\partial A}{\partial t}\right)=0\,. \tag{4}$$

Here, t is the time, z is the longitudinal coordinate, $A(t,z)$ is the envelope of electric field strength related to the intensity by the equation $I=cn_0|A|^2/(8\pi)$, u is the group velocity,

$$u=\left(\frac{\partial\left(kn_0(\omega)\right)}{\partial\omega}\bigg|_{\omega=\omega_0}\right)^{-1},$$

k_2 is the group velocity dispersion,

$$k_2=\frac{\partial^2\left(kn_0(\omega)\right)}{\partial\omega^2}\,,$$

$\omega_0=2\pi c/\lambda_0$ is the central frequency, c is the velocity of light in a vacuum, and $\chi^{(3)}$ is the cubic susceptibility tensor related to the previously introduced nonlinear refractive index n_2: n_2 [cm^2 kW^{-1}] $=(2\pi/n_0)^2\chi^{(3)}$ (in CGSE units) [113]. In the derivation of Eqn (4), it was assumed that the intensity is not high enough to give rise to plasma production and that the pulse duration at the input to the nonlinear medium is much longer than the field cycle.

Equation (4) describes diffraction effects (the term with the transverse Laplace operator ($\Delta_\perp$)), dispersive pulse spreading (the term with the second time derivative), and the effect of Kerr nonlinearity (the terms with $\chi^{(3)}$). Operator $\Delta_\perp$ is important from the standpoint of small-scale self-focusing development (see Section 4) and laser beam diffraction. The group velocity dispersion affects the modification of the pulse envelope. Its net contribution depends on the initial spectral phase modulation and on the relation between the signs of the parameters k_2 and n_2 of the medium. For solid transparent dielectrics, as a rule, k_2 and n_2 are positive in the visible and near-infrared ranges. When the signs are opposite, temporal self-compression is possible in the propagation through the medium (see, for instance, Refs [114–118]). In this review, we will not consider self-compression. Furthermore, Eqn (4) does not include higher orders of dispersion, which result in terms with the third, fourth, etc. time derivatives of A [119], as well as the term [103, 119, 120] with the operator which corrects the slowly varying amplitude approximation and is responsible for spatio-temporal focusing.

The nonstationarity of cubic nonlinearity is disregarded in Eqn (4) (the nonlinearity is assumed to be inertialess), since the response time of the medium is far shorter than the pulse duration. As applied to high-intensity (of the order of several TW cm^{-2}) femtosecond laser pulses propagating in transparent dielectrics, the cubic nonlinearity is due to the manifestation of the anharmonicity of the electronic response of the atoms. The characteristic time scale of nonlinearity relaxation is defined by the electron orbiting period in atoms. For the first Bohr orbit of hydrogen, the period is equal to 0.11 fs. In heavier atoms, this time is longer, but it is nevertheless much shorter than the pulse duration, and so we restrict ourselves to the inertialess nonlinearity case.

Cubic nonlinearity is therefore represented in Eqn (4) by the three terms in parentheses. The first one accounts for the quasistatic response, while the last two describe wave nonstationarity [113]. One can see from Eqn (4) that the last term describes nonlinear dispersion — the intensity dependence of the group velocity — i.e., it is possible to introduce the effective group velocity:

$$u_{\mathrm{eff}}=\frac{u}{1+2n_2I(t)u/c}\,. \tag{5}$$

It follows from formula (5) that the higher-intensity part of a pulse propagates more slowly than the wings in media with $n_2>0$, with the consequential self-steepening of the pulse front resulting in the formation of an envelope shock wave. This circumstance was first pointed out in Ref. [100] and more recently in Refs [121, 122]. Furthermore, the wave nonstationarity may result in the suppression of small-scale self-focusing (see Section 4.4).

2.2 Compression-after-compressor approach (CafCA) in a one-dimensional quasistationary model

We consider the in-medium propagation of laser pulses longer than 10 field cycles, and in this connection we ignore the last two terms in Eqn (4). The corresponding equation was first derived in Ref. [102]. It is also assumed that diffraction effects are weak. Then, Eqn (4) reduces to the equation

$$\frac{\partial a}{\partial Z}-\mathrm{i}\frac{D}{2}\frac{\partial^2 a}{\partial\eta^2}+\mathrm{i}B|a|^2a=0\,, \tag{6}$$

where $Z=z/L$, $\eta=(t-z/u)/T_{\mathrm{F}}$, T_{F} is the half-height duration of a spectrally limited pulse at the input to the nonlinear medium, $a=A(t,z)/A_{10}$, A_{10} is the highest amplitude of the pulse at the input to the nonlinear medium, B is the B-integral (3), and

$$D=L\frac{k_2}{T_{\mathrm{F}}^2}\,. \tag{7}$$

As is clear from Eqn (6), the pulse dynamics are determined by two effects: dispersion (the second term) and nonlinearity (the third term). Parameters B and D characterize these two effects and have a lucid physical meaning: B is the ratio of the medium length L to the nonlinear length (the path length in which the nonlinear phase comes up to unity), and D is the ratio of L to the dispersion length $L_{\mathrm{d}}=T_{\mathrm{F}}^2/k_2$. Note that Eqn (6) has an analytical solution when dispersion is ignored ($D=0$). Moreover, an analytical solution was found for $D=0$ in Ref. [107] even with the inclusion of wave nonstationarity, i.e., when the last two terms of Eqn (4) are returned to Eqn (6).

2.2.1 Spectrally limited pulse. Let us consider the CafCA features in the case of a spectrally limited Gaussian pulse at the input of a nonlinear medium. For this purpose, we will

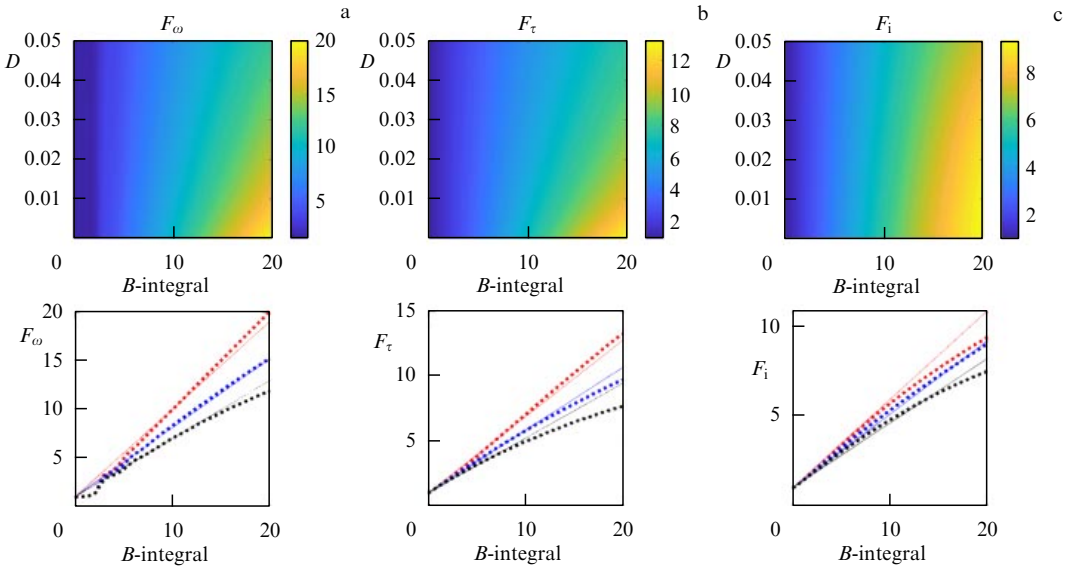

Figure 4. (Color online.) Numerically calculated (a) spectral broadening F_ω, (b) pulse shortening F_τ, and (c) intensity enhancement F_i factors. Dependences in the lower part of the figure were constructed for $D = 0$ (red squares), $D = 0.02$ (blue squares), and $D = 0.05$ (black squares). Solid lines represent Eqn (11).

numerically solve Eqn (6) subject to the boundary condition

$$a(t, Z = 0) = \exp\left(-2\ln 2\,\frac{t^2}{T_F^2}\right). \tag{8}$$

As the pulse propagates through the nonlinear medium, it becomes chirped and its spectrum broadens. Spectral phase correction in the output pulse $a(t, Z = 1)$ permits shortening its duration and increasing its peak intensity. Experimentally available, as a rule, is the correction of only the quadratic spectral phase, which is realized in the reflection from chirped mirrors. This operation is mathematically expressed as follows:

$$a_c(t) = \hat{F}^{-1}\left[\exp\left(-\frac{i\alpha_{opt}\Omega^2}{2}\right)\hat{F}\left[a(t, Z = 1)\right]\right]. \tag{9}$$

Here, $\hat{F}$ and $\hat{F}^{-1}$ are direct and inverse Fourier transform operators, Ω is the detuning from the central frequency, and α_{opt} is the group velocity dispersion parameter of the chirped mirrors, which is selected to maximize the peak intensity of the compressed pulse. Figure 4 shows the dependences of the factors

$$F_\omega = \frac{\Delta\Omega_{out}}{\Delta\Omega_{in}}, \tag{10a}$$

$$F_\tau = \frac{T_F}{T_{out}}, \tag{10b}$$

$$F_i = \frac{I_{out}}{I_{in}}, \tag{10c}$$

which characterize the spectral broadening, the pulse shortening, and the increase in intensity, respectively. Here, $\Delta\Omega_{in} = 4\ln 2/T_F$ and $\Delta\Omega_{out}$ are the half-height spectral widths of the input and output pulses, $T_{in} = T_F$ and T_{out} are their half-height durations, and I_{in} and I_{out} are their peak intensities. Simulations suggest that factors $F_{\omega,\tau,i}$ are independent of the initial pulse duration T_F, provided $\Delta\Omega_{out} < \omega_0/2$. When this condition is violated, the data presented in Fig. 4 cannot be used.

Table 1. Coefficients g and k in Eqn (11).

	F_ω	F_τ	F_i	
			Correction of only quadratic phase	Absolute phase correction
g	0.91 0.88 [233]	0.59	0.49 0.5 [83]	0.54
h	1.5	1.26	1.2	0.75
Range of B values whereby Eqns (11) yield an error under 7% for $D = 0$	6.3 – 28.5	0 – 50	1.6 – 13.5	0 – 20
Range of B values whereby Eqns (11) yield an error under 7% for $D < 0.05$	6.3–17.5	0 – 12	1.6 – 13.5	0 – 13.5

As is seen in Fig. 4, the behavior of $F_{\omega,\tau,i}$ is nicely described by a linear dependence on the B-integral in a wide value range of parameters B and D:

$$F_\omega = 1 + g_\omega B\left(1 - h_\omega\sqrt{D}\right), \tag{11a}$$

$$F_\tau = 1 + g_\tau B\left(1 - h_\tau\sqrt{D}\right), \tag{11b}$$

$$F_i = 1 + g_i B\left(1 - h_i\sqrt{D}\right). \tag{11c}$$

Coefficients g and h, as well as the usable range of Eqns (11), are given in Table 1. The values of F are highest in the absence of dispersion ($D = 0$), i.e., dispersion lowers the efficiency of CafCA. As is clear from Eqns (11), the role of dispersion may be interpreted as the lowering of the effective B-integral value by a factor $(1 - hD^{1/2})$. Notice that the intensity enhancement factor F_i is less affected by dispersion than the other ones. For instance, for $B = 20$, the magnitude of $F_i(D = 0.05)$ is lower than $F_i(D = 0)$ by only a factor of 1.2, while the corresponding factor for F_ω and F_τ is equal to 1.7.

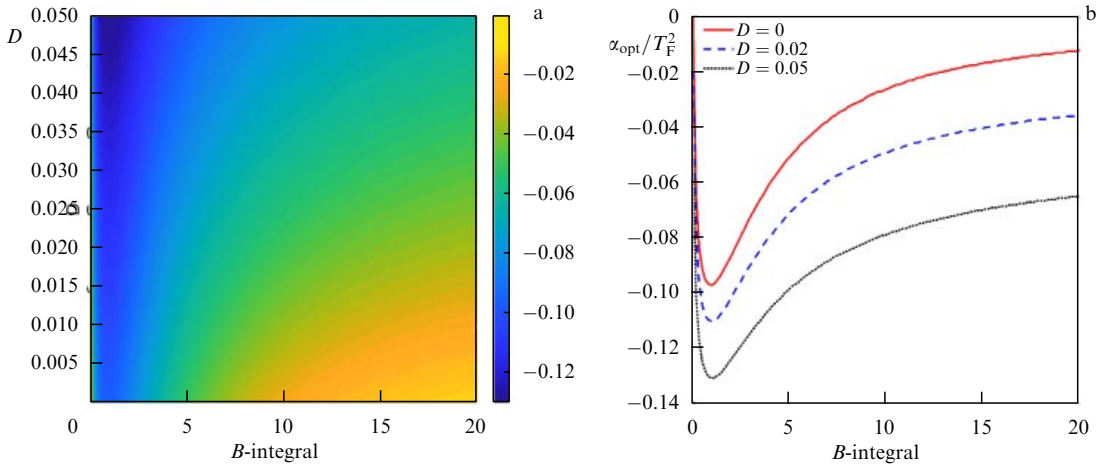

Figure 5. (Color online.) Dependence of chirped mirror dispersion α_{opt}, which is normalized to T_F^2, on B and D. The curves are plotted for $D = 0$ (the red line), $D = 0.02$ (blue), and $D = 0.05$ (black).

Figure 5 shows the B-dependence of parameter α_{opt} normalized to T_F^2 for different D values. As is seen from Fig. 5b, correcting the quadratic spectral phase component for higher values of the B-integral necessitates a lower (in modulus) chirped mirror dispersion α_{opt}. A stronger medium dispersion D requires a stronger dispersion of the chirped mirrors. When the chirped mirror dispersion α is not exactly equal to α_{opt}, F_i is smaller, though insignificantly so. For instance, for $B = 3$, the value of F_i is lowered by less than 10% when α changes from -230 fs^2 to -100 fs^2 [83]. Furthermore, one can see from Fig. 5b that α_{opt} changes only slightly under B-integral fluctuations. Therefore, errors in the fabrication of the mirrors and the instability of laser parameters have a moderate effect on the CafCA efficiency.

If we do not restrict ourselves to the correction of only the quadratic spectral phase component and realize an absolute correction, i.e., make constant the phase of the output pulse, F_i will be greater. However, the difference is slight — about 10% (compare the coefficients in the last two columns in Table 1). Numerical simulations for $B = 48$ has shown [87] that even for this extremely high B value the difference in F_τ amounts to only 20%.

2.2.2 Chirped pulse. Let the laser pulse possess a linear frequency modulation (which corresponds to a parabolic spectral phase) at the input boundary of a nonlinear element:

$$a(t, Z = 0) = \hat{F}^{-1}\left[\text{const}\,\exp\left(-2\ln 2\,\frac{\Omega^2}{\Delta\Omega_{in}^2} - i\,\frac{1}{2}\,\alpha_{in}\Omega^2\right)\right]. \quad (12)$$

The duration T_{in} of this pulse is determined by the chirp magnitude α_{in} and the duration T_F of the spectrally limited pulse of spectral width $\Delta\Omega_{in}$:

$$T_{in} = T_F\sqrt{1 + \left(\frac{4\alpha_{in}\ln 2}{T_F^2}\right)^2}.$$

Using this notation, the negative (positive) sign of parameter α_{in} corresponds to the negative (positive) linear frequency modulation. Long-wavelength spectral components propagate at the leading pulse edge for a positive frequency modulation and the short-wavelength components for a negative one. For a fixed pulse energy, the introduction of

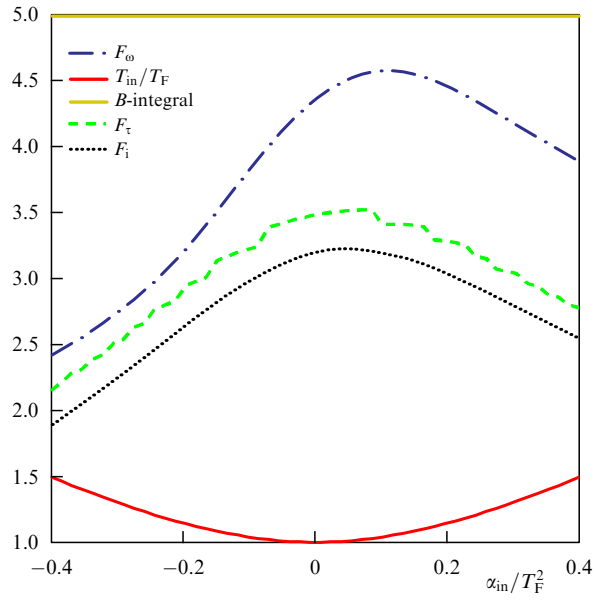

Figure 6. (Color online.) Dependences of F_ω, F_τ, F_i, B, and T_{in}/T_F on parameter α_{in}.

phase modulation (irrespective of its sign) entails a lowering of the peak intensity and the B-integral by a factor T_{in}/T_F.

The sign of α_{in} affects the behavior of F_ω, F_τ, and F_i. We consider this issue in greater detail. For a more correct comparison, we assume that the introduction of frequency modulation into the initial pulse does not change the magnitude of the B-integral, e.g., due to a change in pulse energy. Figure 6 shows the dependences of parameters F_ω, F_τ, F_i, and T_{in}/T_F on parameter α_{in} calculated for $D = 0.02$ ($k_2 > 0, n_2 > 0$) and $B = 5$. Equation (6) was solved with boundary condition (12). As is clear from Fig. 6, the positive chirp in the input pulse has only a slight effect on the spectral broadening coefficient F_ω, while the negative one, on the contrary, strongly decreases it. The asymmetry in the behavior of dependences $F_\tau(\alpha_{in})$ and $F_i(\alpha_{in})$ is much weaker. Figure 7 shows the two-dimensional distribution of F_i as a function of the B-integral and parameter $\alpha_{in}(T_F)^{-2}$ for $D = 0.02$. When the initial pulse is chirped, an increase in B-integral entails, as before, an increase in the peak intensity

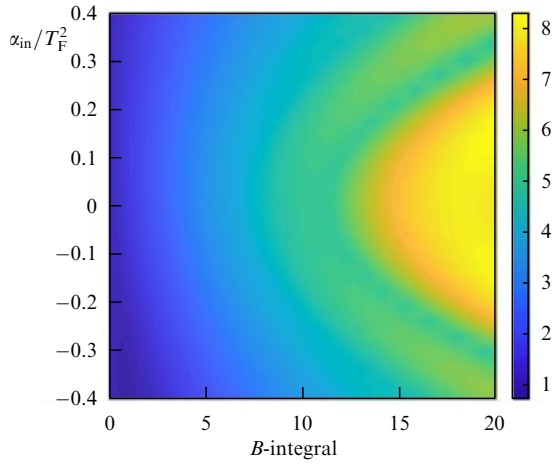

Figure 7. (Color online.) Coefficient F_i as a function of the B-integral and parameter α_{in}/T_F^2 for $D = 0.02$.

after compression. The greatest increase is observed for pulses with a small ($\alpha_{in} = 0.14T_F^2$) positive frequency modulation. However, in this case, the maximum values of factors F_ω, F_τ, and F_i are only slightly higher than those for $\alpha_{in} = 0$ (see Figs 6 and 7). That is why for the experimental implementation of CafCA it is expedient to employ spectrally limited pulses, or nearly such. At the same time, even in the presence of a significant chirp $|\alpha_{in}| = 0.4T_F^2$, whereby the pulse duration is 1.5 times longer than the Fourier limit, CafCA affords more than a six-fold increase in intensity for $B = 20$ (see Fig. 7).

2.2.3 Effect of third- and fourth-order spectral phase. As shown in Section 2.2.2, there is good reason to nullify the quadratic spectral phase to make the CafCA operation efficient. This is fairly simple to do by stretcher or compressor alignment. In this section, we assume that $\alpha_{in} = 0$ and consider the effect of the third- and fourth-order frequency terms in the spectral phase of the input pulse exerted on F_ω, F_τ, and F_i. For a boundary condition for Eqn (6), we take

$$a(t, Z = 0) = \hat{F}^{-1}\left[\text{const}\,\exp\left(-2\ln 2\,\frac{\Omega^2}{\Delta\Omega_{in}^2} - \mathrm{i}\,\frac{1}{6}\,\beta\Omega^3 - \mathrm{i}\,\frac{1}{24}\,\gamma\Omega^4\right)\right]. \quad (13)$$

First of all, we note that high values of β or γ result in a qualitatively different spectral broadening: narrow peaks appear in the spectrum, while the broadening becomes smaller, which was shown theoretically and borne out experimentally in Ref. [83]. These spectral features are clearly demonstrated in Fig. 8. The spectra shown in Fig. 8 depend only slightly on the magnitude of medium dispersion for $0 < D < 0.05$. The picture varies insignificantly for this D range.

Introducing aberrations in the spectral phase lowers the peak intensity. We consider the ranges of β/T_F^3 and γ/T_F^4 parameter variation, such that the introduction of only one of the terms under consideration results in a 20% lowering of the peak intensity. To make the comparison more correct (such as was done in Section 2.2.2), we assume that the introduction of phase modulation does not change the magnitude of the B-integral, e.g., due to an increase in pulse energy.

Figure 9 shows the two-dimensional diagrams of spectral broadening F_ω, pulse shortening F_τ, and peak intensity enhancement F_i factors for $D = 0.02$ and $B = 5$ ($k_2 > 0, n_2 > 0$). These factors are highest in the absence of the cubic term, i.e., for $\beta = 0$, these distributions being symmetrical with respect to the sign of β. At the same time, the greatest spectral broadening, duration shortening, and peak intensity enhancement occur for $\gamma > 0$. The fourth-order frequency aberrations of the spectral phase affect F_ω, F_τ, and F_i in a similar way as the effect of the parabolic spectral phase (see Section 2.2.2). It is significant that the magnitude of optimal chirped mirror dispersion α_{opt} varies only slightly, even though it depends on β and γ: the total variation range is less than 18% from the average value $\alpha_{opt} = -0.08T_F^2$.

We note that spectral broadening F_ω varies significantly in the range of β and γ values under consideration (Fig. 9a). In this case, the duration and peak intensity of the compressed pulse differ by less than 22% from their optimal values (Figs 9b, c). Factors F_ω, F_τ, and F_i show a close-to-linear dependence (11) on the B-integral (see also Ref. [80]). Therefore, pulses with the third- and fourth-order frequency terms in the spectral phase may be compressed using CafCA almost as efficiently as spectrally limited pulses.

2.3 Special features for pulses several hundred femtoseconds in duration

Of special interest is the use of CafCA at the output of petawatt neodymium glass lasers. The most striking exam-

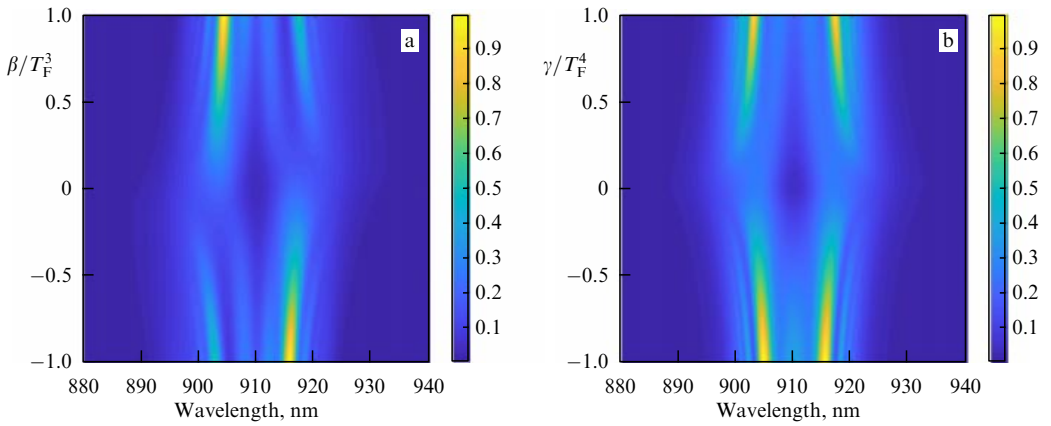

Figure 8. (Color online.) Pulse spectra after passage through a nonlinear medium with $B = 5$, $D = 0.02$ calculated depending on the phase aberrations (a) β/T_F^3 and (b) γ/T_F^4 at the input to the nonlinear medium.

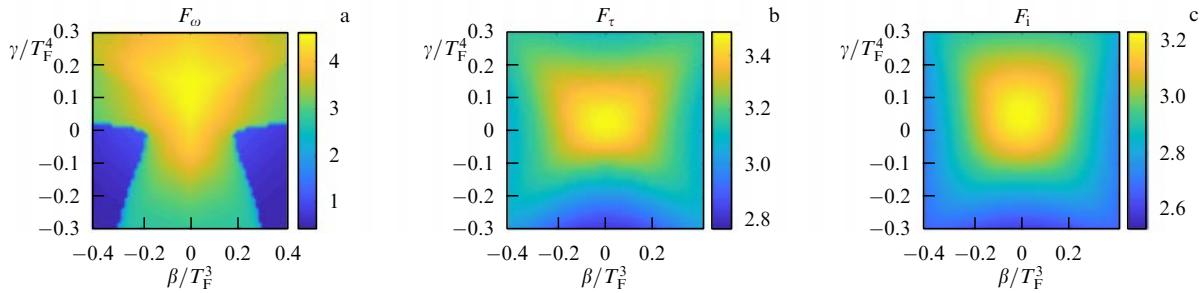

Figure 9. (Color online.) Factors (a) F_ω, (b) F_τ, and (c) F_i shown as functions of the phase aberrations β/T_F^3 and γ/T_F^4 for $D = 0.02$ and $B = 5$.

ples are the Texas Petawatt Laser [123], the French complex PETawatt Aquitaine Laser system (PETAL) [124, 125], and the German Petawatt High-Energy Laser for heavy Ion eXperiment (PHELIX) [126]. The output pulses of these systems are almost spectrally limited and have a rather long duration — several hundred femtoseconds — and a high energy level — several hundred or thousand joules. In this case, the peak intensity at the output of the compressor lies in the range of 1–10 TW cm^{-2} [21], as with the output beams of petawatt lasers using parametric amplifiers [127–129] and/or amplification in a Ti:sapphire. The mathematical model of CafCA suggests that the efficiency of additional time compression depends little on the duration and energy of the pulses and that, generally, the previously drawn conclusions still stand. Some differences do, nevertheless, exist.

First of all, an increase in the initial pulse duration by an order of magnitude also increases by an order of magnitude the maximum possible factor F_τ of compression in time, since the shortest duration of a compressed pulse is limited, as before, by the optical field cycle. From this standpoint, the use of CafCA for long pulses is more attractive than for short ones. As shown in Section 5.3, there is good reason to employ two-stage (or even multistage) compression to attain very high compression factors F_τ. Another advantage of long pulses is the extremely weak influence of the linear dispersion of the medium, since parameter D is inversely proportional to the square of T_F (7), and the smallness of D is among the necessary conditions for efficient CafCA application.

At the same time, there are unfavorable aspects as well. Phase correctors with a high group velocity dispersion α_{opt} are required, since parameter α_{opt} is also proportional to the square of T_F (see Fig. 5). With the use of dispersive mirrors, this fact may turn out to be critical, since attaining high α_{opt} values necessitates using many dielectric layers, which complicates the fabrication of mirrors and lowers their surface radiation resistance. Furthermore, in the development of self-focusing (see Section 4), for a long pulse the breakdown probability becomes higher due to a free-electron avalanche, since the time for its formation becomes longer.

To date, CafCA has been tested with long pulses at only the millijoule level [71]. Numerical simulations [79] have borne out the promise of using CafCA for PETAL (see Section 6.2).

2.4 Special features for pulses shorter than 15 fs

The additional compression of initially very short pulses (15 fs in duration and shorter) is of major interest from the viewpoint of producing high-power pulses of extremely short duration — about one optical field cycle. There is no fundamental difference from the compression of longer pulses, but there are some special features related to the propagation of ultrashort pulses in a nonlinear medium. Let us discuss them.

First, the terms responsible for the wave nonstationarity should be taken into account in Eqn (4). Recall that these terms are related to the time dependence of nonlinear polarization. Their inclusion entails a distortion of the pulse shape due to the intensity dependence of the group velocity and an asymmetric spectral broadening [20, 113].

Second, the role of dispersion rises in importance (D is proportional to k_2/T_F^2 (7)), and therefore media with a low group velocity dispersion k_2 are required. To decrease the nonlinear element thickness L for a given value of the B-integral requires media with high n_2 and/or high intensities I. The increase in intensity is limited by an optical breakdown and plasma production. Therefore, the ratio n_2/k_2 is the figure of merit of a nonlinear medium from the standpoint of applying CafCA to ultrashort pulses. The higher-order dispersion terms omitted in Eqn (4) may turn out to be significant for very short pulses [119].

Third, for short pulses, it is necessary to distinguish the cases of oblique and oblique incidence on a nonlinear element. In the case of normal incidence, in a medium with frequency dispersion due to a difference between the group and phase velocities, the amplitude and phase fronts do not coincide and, as a consequence, a transverse group delay appears, and the refracted pulse becomes spatially nonuniform. For very short pulses, the time delay may be comparable to their duration [113]. To state it in different terms, the refracted pulse acquires a tilt of the amplitude front and its related angular chirp, which should be included in the initial condition at the media interface. To elucidate how this affects the compression results described above is the subject of future investigations.

Fourth, the requirements imposed on the parameters of dispersive mirrors change significantly. On the one hand, broader-band mirrors are required, which complicates their fabrication, and on the other hand, their dispersion α_{opt}, which is proportional to the square of T_F, becomes significantly lower, which, conversely, facilitates their fabrication.

A new approach is promising for short pulses, which has recently gained wide acceptance. It abandons the approximation of slowly varying amplitudes, i.e., abandons Eqn (4). In the framework of this approach, the field dynamics are described in the so-called reflectionless approximation, without a scale-based division into a slow envelope and a high-frequency carrier. (For more details, the reader is referred to Refs [109, 110, 120, 130–133] and references therein.)

There are no experimental data on applying CafCA to pulses shorter than 30 fs, and this is a subject for future research. An example of numerical simulation [79] is given in Section 6.2.

3. Compression nonuniformity over beam cross section

As stated in the Introduction, in free laser beam propagation through a nonlinear element, there inevitably arise problems related to the spatial nonuniformity of the beam. We restrict ourselves to a consideration of an axially symmetric case: $I = I(r)$. Typical for lasers of moderate power (1–10 TW) is the Gaussian intensity distribution, while the beams of ultrahigh-power lasers (0.1–10 PW) are closer to flat-top ones. It is therefore evident that the indicated parasitic effects become less significant with an increase in power. For a qualitative description, the initial laser pulse is conveniently defined in the form of a super-Gaussian function of radius w and order m:

$$a(t=0, z=0, r) = \exp\left(-\frac{r^{2m}}{2w^{2m}}\right),$$
$$I_{\text{in}}(r) = I\exp\left(-\frac{r^{2m}}{w^{2m}}\right). \tag{14}$$

Parameter m describes the degree of beam nonuniformity: for $m = 1$, formula (14) describes a Gaussian beam and for $m = \infty$ a flat-top one. The spatial beam nonuniformity has the effect that, according to Eqns (3) and (14), the nonlinear phase incursion — the B-integral — is also a function of r. This leads to three parasitic effects: self-focusing of the beam as a whole (i.e., large-scale self-focusing), nonlinear phase aberrations, and, most importantly, nonlinear spectral broadening and the consequential nonuniform pulse compression. We note that in a single-mode fiber the nonlinear phase is added to the entire mode, i.e., to the entire beam, and all these effects are absent. We consider these three parasitic effects and the methods for their suppression.

3.1 Large-scale self-focusing

Large-scale self-focusing (LSSF) — the focusing of a beam as a whole — occurs when the beam power exceeds the critical self-focusing power P_{cr}. The physical meaning of P_{cr} is very simple: this is the power at which diffraction beam spreading is compensated by its self-focusing. For a Gaussian beam, $P_{\text{cr}} = 0.174\lambda^2/(n_2 n_0)$ [134]. However, the condition $P > P_{\text{cr}}$ (and even $P \gg P_{\text{cr}}$) by no means implies that the LSSF and beam collapse will occur: for the collapse of the beam as a whole to occur, the path of beam propagation in the nonlinear medium must be long. Its length L_{LSSF} was numerically found in Ref. [134]:

$$\frac{L_{\text{LSSF}}}{kw^2} \approx \frac{0.37}{\sqrt{\left(\sqrt{P/P_{\text{cr}}} - 0.825\right)^2 - 0.03}}. \tag{15}$$

Typical P_{cr} values in a solid are equal to several MW, i.e., are many orders of magnitude lower than the power of an ultrahigh-power laser, and L_{LSSF} for $P \gg P_{\text{cr}}$ is proportional to $(P_{\text{cr}}/P)^{1/2}$, which was first pointed out in Ref. [135]. This gives rise to the wrong belief that LSSF is an extremely dangerous effect. In reality, it is quite to the contrary: LSSF is not a problem for ultrahigh-power laser beams. Considering that $P \gg P_{\text{cr}}$ and $P = \pi w^2 I$, formula (15) is easily brought to the form

$$\frac{L_{\text{LSSF}}}{L} \approx \text{const}\left(\frac{w}{\sqrt{L\lambda}}\right)^3, \tag{16}$$

where const $\approx 1.4(Bn_0)^{-1/2}$ is a factor of the order of unity. Hence, it is clear that $L_{\text{LSSF}} \gg L$ for beams 1 mm in diameter and over, i.e., that LSSF is ruled out even for a Gaussian beam. In other words, in the SPM, the diameter and shape of the beam of an ultrahigh-power laser remain invariable in the propagation in a nonlinear element. For a more uniform super-Gaussian beam, the effect is even weaker and may all the more be ignored.

3.2 Nonuniform pulse shortening

The most important problem of CafCA for spatially nonuniform beams is the fact that the spectral broadening due to SPM and, as a consequence, the duration and intensity of the compressed pulse are different at different points of the cross section. To state it in other words, at the beam periphery, the spectral broadening and the increase in intensity are significantly smaller than on the beam axis, where the B-integral attains its maximal value $B(r = 0)$. As a result, the increase in pulse power is smaller than for a flat-top beam, which is described by Eqns (11). In many papers [35, 65–68, 74], this problem is indicated as the main limitation for the SPM in free beam propagation in a nonlinear medium.

In Section 3.2.1, we consider the issue of how the CafCA efficiency depends on the beam shape, namely on parameter m. Section 3.2.3 is concerned with the method of solving this problem, which involves the use of a negative lens as a nonlinear medium.

3.2.1 Dependence of compression on the beam shape. Using expression (11c) to increase intensity F_{i}, it is possible to obtain the power enhancement factor $F_{\text{p}} = P_{\text{out}}/P_{\text{in}}$ by integrating F_{i} over the cross section of a super-Gaussian beam (14):

$$F_{\text{p}} = \frac{\int_0^\infty F_{\text{i}} \exp\left(-r^{2m}/w^{2m}\right) r\,\text{d}r}{\int_0^\infty \exp\left(-r^{2m}/w^{2m}\right) r\,\text{d}r} = 1 + g_{\text{i}} B\left(1 - h_{\text{i}}\sqrt{D}\right) 2^{-1/m}. \tag{17}$$

Comparing expressions (17) and (11c) shows that the beam nonuniformity is equivalent to the lowering of the B-integral by $2^{1/m}$ times. For a flat-top beam ($m = \infty$), $F_{\text{p}} = F_{\text{i}}$, while for a Gaussian beam ($m = 1$), $F_{\text{p}} = 0.5F_{\text{i}}$, i.e., for $B \gg 1$, the increase in Gaussian beam power may nevertheless be significant. For a super-Gaussian beam with a high m, the increase in power for CafCA is practically the same as the increase in intensity. For instance, for $m = 4$, $F_{\text{p}} \approx 0.92F_{\text{i}}$. A similar result is obtained by averaging expressions (11b, c) over the cross section: F_ω and F_τ will decrease by a factor $2^{1/m}$.

We note that the above reasoning for F_{p} and F_τ disregards the fact that Eqns (11b, c) were obtained with the inclusion of optimal mirror dispersion ($\alpha = \alpha_{\text{opt}}$) for each value of the B-integral. In reality, the value of α cannot change from point to point of the cross section. Strictly speaking, integration should be performed not of Eqns (11) but of the corresponding coefficients obtained for one value of α. It is evident that factors F_{p} and F_τ will be lower in this case. At the same time, the dependence of α_{opt} on the B-integral is smooth, especially so in the most interesting range $B \gg 1$ (see Fig. 5), and so this error is insignificant.

3.2.2 Uniform compression with a negative lens. As is clear from expression (17), for a Gaussian beam, $F_{\text{p}} = F_{\text{i}}/2$, i.e., the resultant beam power is one half that for a flat-top beam. This 'half' was first obtained numerically in Ref. [35]. To make up for this 'half', it was proposed in [89, 136] to employ for SPM

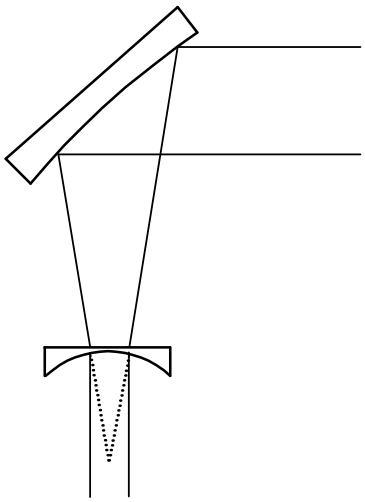

Figure 10. Schematic representation of quasi-uniform *B*-integral accumulation by Gaussian beams.

a nonlinear element in the form of a negative lens instead of plane-parallel plate. Figure 10 serves to illustrate this idea. The lens parameters are selected to minimize for every ray the deviation of the product *IL* of intensity and nonlinear-medium length from the constant value. This minimizes the variations in the *B*-integral (3). An off-axis parabolic mirror collimates the laser beam. As a result, the beam retains a plane wave front and a Gaussian intensity profile and accumulates the *B*-integral, which is quasi-uniform over the beam cross section. The proposed scheme received the name 'nonlinear telescope'. The laser radiation is next delivered to dispersive mirrors. (For more details, see Ref. [89].)

The scheme described above was first tested in experiments on the Advanced Laser Light Source (ALLS) in Canada [77]. The pulses had a quasi-Gaussian spatial intensity distribution, a central wavelength of 800 nm, an intensity full width at half maximum (FWHM) duration of 40–45 fs, a beam diameter of 7.4 mm at a level e^{-2}, and an energy of up to 28 mJ. A defocusing lens made of TF12 glass of on-axis thickness 0.2 mm was employed for spectrum broadening. The respective focal lengths of the lens and the parabolic mirror were equal to −20.7 mm and 50 mm. The spectral broadening was practically the same for different domains of the transverse quasi-Gaussian intensity distribution. It was possible to demonstrate duration shortening from 45 fs to 20 fs for the central beam region and to 29 fs at 7 mm from the center.

In Ref. [78], the energy and diameter of the laser beam were significantly increased: 170 mJ and 38 mm at a level of $1/e^2$, respectively. The peak intensity of 33-fs-long pulses was equal to 836 GW cm^{-2}. For a nonlinear element, use was made of a plano-concave lens of TF12 glass with an on-axis thickness of 0.3 mm. After passing through a nonlinear telescope, the laser beam measured 52 mm at a level $1/e^2$. To suppress small-scale self-focusing, use was made of beam self-filtering in the free-space propagation (see Section 4.3). The pulse shapes and durations at different points of the beam are presented in Fig. 11. As is evident from Fig. 11a, there is an insignificant postpulse for all measured transverse positions, which is due to the residual uncompensated higher-order phase. One can see from Fig. 11b that the duration of a compressed pulse ranges between 16 and 18 fs in a domain broader than 17.5 mm. The pulse duration in Fig. 11b is asymmetric about the beam center, because the distribution used in the experiments was different from the Gaussian one. Therefore, a laterally quasi-uniform two-fold duration shortening was demonstrated with the use of a nonlinear telescope and a system of chirped mirrors.

3.3 Nonlinear wavefront distortions

In the propagation through a nonlinear element, a laser beam acquires nonlinear phase distortions (aberrations) defined by the phase Ψ, which is proportional to the intensity. In view of expressions (3) and (14), we obtain

$$\Psi(r) = B\exp\left(-\frac{r^{2m}}{w^{2m}}\right). \tag{18}$$

Here, B is the on-axis B-integral value. Near the beam axis, Ψ is proportional to r^2, and the aberrations are therefore conveniently divided into two parts: parabolic and nonparabolic. The former are characterized by the focal length f of a 'nonlinear lens' (for $n_2 > 0$, the lens is positive, i.e., $f > 0$), and they can be easily compensated by an ordinary negative lens of focal length $-f$. In this case, in the beam there persists the phase

$$\Psi_{\rm comp}(r) = B\exp\left(-\frac{r^{2m}}{w^{2m}}\right) + \frac{kr^2}{2f}. \tag{19}$$

In practice, the negative lens may be omitted: it would suffice to take into account that the 'nonlinear lens' shortens the distance of the beam waist from the focusing parabola. In this case, the focal spot diameter and the intensity of focused

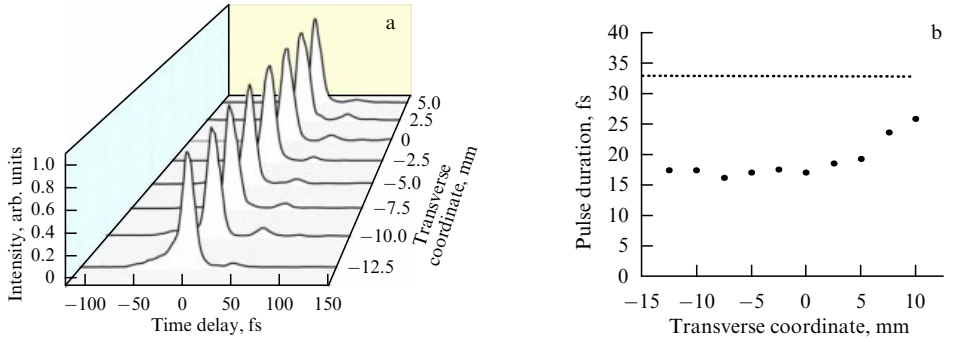

Figure 11. Experimental data of Ref. [78]: (a) pulse shapes at different points of the cross section; (b) dependence of pulse duration on the transverse coordinate (circles); the dotted line stands for the initial pulse duration.

radiation remain invariable. Nonparabolic aberrations, by contrast, are extremely hard to compensate, and they entail a decrease in the at-focus intensity.

Nonlinear beam aberrations were qualitatively analyzed in Ref. [137]. To quantify the strength of aberrations, use is most often made of the M^2 parameter [138] and the Strehl number [139]. Parameter M^2 shows by how many times the beam divergence exceeds that of a Gaussian beam with a plane front. Parameter M^2 is convenient to calculate using formulas from Ref. [140] obtained by the moments method [141]. We will use the quantity μ:

$$\mu = \left(\frac{M^2(\Psi = 0)}{M^2(\Psi)}\right)^2 , \tag{20}$$

which, in view of formula (1), is approximately equal to the lowering of focal intensity I_{focus} in comparison with the nonaberrated beam intensity. The strength of aberrations is more informative to characterize by the Strehl number S, which, by definition, is equal to the lowering of the focal intensity I_{focus} on the beam axis:

$$S = \frac{I_{\text{focus}}(r = 0, \Psi = \Psi_{\text{comp}})}{I_{\text{focus}}(r = 0, \Psi = 0)} , \tag{21}$$

i.e., the focal intensity enhancement factor F_{focus} is defined as

$$F_{\text{focus}} = SF_{\text{p}} . \tag{22}$$

Parameter M^2 and, hence, μ remain invariable when a parabolic phase is introduced into the beam, i.e., they do not depend on whether the parabolic aberrations are compensated or not, while the Strehl number S, by contrast, does depend on it. When calculating the Strehl number by formula (21), we assume that the parabolic part of the aberrations is compensated. For small aberrations ($\Psi_{\text{comp}} \ll 1$), Perevezentsev et al. [142] obtained formulas for calculating f, μ, and S:

$$\frac{kw^2}{f} = B\frac{2\Gamma(2/m)\Gamma(1/m)}{\Gamma(3/m)\Gamma(1/m) - \Gamma(2/m)\Gamma(2/m)}\frac{3^{-1/m} - 9^{-1/m}}{2^{1/m}} , \tag{23}$$

$$\mu = 1 - B^2\left(\frac{4}{9} - 4^{-1/m}\frac{\Gamma(1/m)\Gamma(1/m)}{m^2\Gamma(2/m)}\right) , \tag{24}$$

$$S = 1 - B^2\left\{5^{-1/m} - 9^{-1/m} - \frac{\left[\Gamma(2/m)(2^{-1/m} - 4^{-1/m})\right]^2}{\Gamma(3/m)\Gamma(1/m) - \Gamma(2/m)\Gamma(2/m)}\right\} , \tag{25}$$

where $\Gamma(x)$ is the gamma function. Therefore, f, μ, and S depend on two parameters: the B-integral, which characterizes the measure of nonlinearity, and parameter m, which characterizes the beam nonuniformity. The right-hand side of Eqn (23) is close to unity by the order of magnitude (for a Gaussian beam, it is equal to $0.22B$). So, the focal length of the 'nonlinear lens' is of the order of the Rayleigh length $kw^2/2$, i.e., for beams of diameter $2w > 20$ mm we obtain $f > 300$ m. However, this does not mean that the nonlinear aberrations may be disregarded.

One can see from expression (23) that f also tends to infinity for $m = \infty$: a flat-top beam also acquires a planar nonlinear phase, i.e., it is free from any aberrations. At the same time, parameter μ (24) tends to $1 - 4B^2/9$ rather than to unity, i.e., 'indicates' that there are aberrations and the nonlinear phase increases parameter M^2. The reason for this nonphysical conclusion is that parameter M^2 for super-Gaussian beams with a high m is significantly different from unity even for a plane wavefront ($\Psi = 0$). Furthermore, parameter M^2 tends to infinity for a flat-top beam and its use is basically incorrect [140, 143]. Strehl number S, like parameter M^2, signifies that the strongest aberrations appear in a Gaussian beam ($m = 1$). Unlike μ, Strehl number S, as is evident from expression (25), tends to unity when $m = \infty$. But the convergence is very slow, and even for $m = 20$ it is appreciably different from unity, especially so for large B (Fig. 12). At the same time, the dependence $S(m)$ is nonmonotonic: for $B < 5$, there is an optimal value $m_{\text{opt}} = 3$, which minimizes aberrations. Moreover, even for $m = 2$, the S values are only slightly smaller than $S(m = 3)$. Proceeding from expression (24), it is readily shown that μ also peaks for $m = 2-3$. This nonmonotonic dependence of aberrations on m is explained as follows. With increasing m, on the one hand, the phase distortions displace towards the beam periphery and, on the other hand, the fraction of parabolic distortions becomes smaller and the fraction of nonparabolic ones becomes significantly larger, because the total nonlinear phase difference between the axis and the beam boundary is equal to B, irrespective of the m value. Therefore, there is no need to aim for large m values. It is quite sufficient to have $m = 2-3$, and for $B < 6$ the Strehl number $S > 0.8$, i.e., aberrations will result in the lowering of focal intensity by no more than 20%.

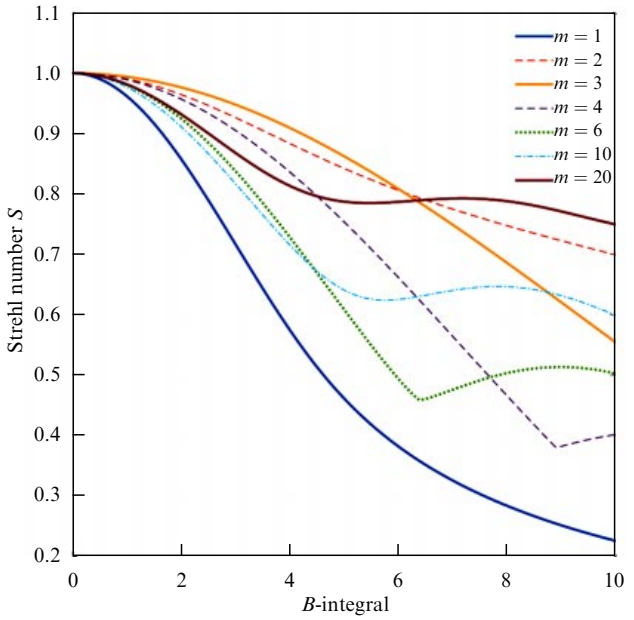

Figure 12. (Color online.) Dependence of the Strehl number S on the B-integral for different values of m.

For a Gaussian beam and a super-Gaussian one with $m = 5-8$, the lowering of focal intensity is quite significant, especially so for large B. In cases where this is unacceptable, it is necessary to employ an adaptive mirror, which may be placed either in front of or behind CafCA. The amplitude of phase distortions is equal to B, i.e., even for $B = 12.6$, the distortions amount to only two wavelengths, which is quite amenable to amendment by modern adaptive mirrors [144, 145]. We also note that adaptive mirrors are employed in many modern lasers, and in this case it is only required to modify their control software.

4. Small-scale self-focusing of ultrahigh-power laser beams

As shown in Section 3, the larger the temporal pulse compression factor, the stronger the manifestation of the parasitic effects caused by the nonuniformity of a laser beam. This connection may be severed without 'throwing the baby out with the bathwater' using the methods of linear optics. Small-scale self-focusing (SSSF) is responsible for the growth of the amplitude of harmonic perturbations of a plane wave in a medium with a cubic nonlinearity. The simplest model of instability growth was first presented by Bespalov and Talanov [90]. Due to SSSF manifestation, the beam splits into a multitude of filaments, which significantly impair its quality and eventually result in the breakdown of optical elements. Unlike nonlinear phase aberrations (see Section 3.3), the acquired distortions are impossible to decrease by external devices like adaptive mirrors, and therefore the only possibility of fighting them is to bar its development.

The instability increment is determined by the B-integral (3) and, as a rule, a beam splits into filaments for $B > 2-3$. One and the same parameter — the B-integral — is simultaneously useful and parasitic. On the face of it [72, 74, 88, 93], for this reason the implementation of CafCA is possible only in a narrow range, $B < 3$, which permits figuring on only a 2–2.5-fold increase in power, even theoretically (see Section 2). In Section 4.1, we summarize the results of the linear SSSF theory, which was developed in the 1960s–1980s as applied to neodymium glass nanosecond lasers. In comparison with SSSF in these lasers, SSSF in ultrahigh-power femtosecond lasers shows significant differences (see Section 4.2), making it possible to apply a new method to suppress it — self-filtering of the beam (see Section 4.3). Other SSSF suppression techniques and the prospects of using them for CafCA are discussed in Sections 4.4 and 4.5.

We emphasize that all these methods permit suppressing SSSF in any pass-through optical elements placed in high-power femtosecond beams, for instance, in frequency doublers, $\lambda/4$ and $\lambda/2$ plates, beam splitters, and screens used for the protection of optical devices from the plasma ejected from the target.

4.1 Theory of small-scale self-focusing

SSSF is the spatial instability of a plane wave propagating in a medium with a cubic nonlinearity — a growth of the amplitude of spatial harmonic perturbations. The SSSF theory foundations were laid by Bespalov and Talanov in Ref. [90], and the instability is termed modulation or Bespalov–Talanov instability. The theory was further developed in a number of papers [146–157]. An alternative interpretation of the instability reliant on the concept of stimulated four-wave interaction was developed in Refs [158, 159].

The first experimental confirmation of the theory [90] was obtained by Yu Chilingaryan [160], who investigated SSSF in liquids. The measurements were in quantitative agreement with predictions [90] and confirmed the qualitative difference between SSSF and large-scale self-focusing. More recently [161–164], experimental data were obtained which also bore out the theory. Theoretical and experimental SSSF research is still underway [93, 165–172].

Below, we briefly describe the results of the SSSF theory, which are critically important for understanding the SSSF in ultrahigh-power femtosecond lasers. The instability of a plane wave is described in the framework of the dispersion-free stationary approximation, under which Eqn (4) reduces to

$$\frac{\partial a}{\partial Z} - \frac{\mathrm{i}L}{2k}\,\Delta_\perp a + \mathrm{i}B|a|^2 a = 0\,. \tag{26}$$

Added to the solution of Eqn (26) in the form of a plane wave $a(Z) = \exp(-\mathrm{i}BZ)$ is perturbation (noise) in the form $a_1(Z)\exp(\mathrm{i}\varphi_{\mathrm{in}}(Z))\cos(k_\perp x)$, which is a pair of plane waves with a low amplitude ($a_1 \ll 1$) and an arbitrary transverse wavevector $k_\perp$ ($k_0 = 2\pi n_0/\lambda_0$) propagating at an angle $\theta = \pm k_\perp/k_0$ to the z-axis. From this point on, the lowercase letter θ denotes angles inside the nonlinear medium, and the capital letter Θ the angles outside of it. An arbitrary perturbation may be represented in the form of a superposition of such waves. As shown in Ref. [90], the perturbations may be unstable for

$$0 < \kappa < \kappa_{\mathrm{cr}} = 2\sqrt{B}\,, \tag{27}$$

where κ is the dimensionless transverse wavenumber,

$$\kappa = k_\perp\sqrt{\frac{L}{k_0}}\,. \tag{28}$$

The instability increment attains its maximum for

$$\kappa_{\max} = \frac{\kappa_{\mathrm{cr}}}{\sqrt{2}} = \sqrt{2B}\,. \tag{29}$$

We note that $\kappa_{\max}$ is defined only by the B-integral. The perturbations with $\kappa = \kappa_{\max}$ are the most dangerous from the standpoint of SSSF development. Accordingly, the most dangerous angle $\theta_{\max}$ is defined by the formula

$$\theta_{\max} = \frac{\theta_{\mathrm{cr}}}{\sqrt{2}} = \sqrt{\frac{2n_2 I}{n_0}} \tag{30}$$

and is independent of the length of the nonlinear medium. In Refs [154, 155], the complex perturbation amplitude is represented in the form of a real vector

$$\boldsymbol{\varepsilon} = \begin{pmatrix} b\cos\varphi_{\mathrm{in}} \\ b\sin\varphi_{\mathrm{in}} \end{pmatrix}, \tag{31}$$

and an expression is derived for the transmission matrix U, which permits finding the output perturbation amplitude $\boldsymbol{\varepsilon}_{\mathrm{out}} = U\boldsymbol{\varepsilon}_{\mathrm{in}}$:

$$U = \begin{pmatrix} \cosh(Bx) & -\dfrac{\kappa^2}{2Bx}\sinh(Bx) \\ -\dfrac{2Bx}{\kappa^2}\sinh(Bx) & \cosh(Bx) \end{pmatrix}. \tag{32}$$

Here,

$$x^2 = 4\left(\frac{\kappa^2}{\kappa_{\mathrm{cr}}^2} - \frac{\kappa^4}{\kappa_{\mathrm{cr}}^4}\right) = 4(\xi - \xi^2)\,, \tag{33}$$

where $\xi = (\kappa/\kappa_{\mathrm{cr}})^2$. When condition (27) is violated, x becomes an imaginary quantity, but transmission matrix (32) remains real, and it may be used for arbitrary κ. From matrices (31) and (32), it is easy to obtain the noise power gain coefficient $K = |\varepsilon_{\mathrm{out}}/\varepsilon_{\mathrm{in}}|^2$ and the noise phase φ_{out} at the

Table 2. Noise gain.

Input noise phase φ_{in}	K	$K(\kappa=\kappa_{max})$	$K(\kappa=\kappa_{cr})=K(\kappa=0)$
Arbitrary	(34)	$\exp(2B)-[1+\sin(2\varphi_{in})]\sinh(2B)$	$1+4B^2\cos^2\varphi_{in}-2B\sin(2\varphi_{in})$
$\varphi_{in}=0$ (amplitude noise)	$\cosh^2(Bx)+\frac{4B^2x^2}{\kappa^4}\sinh^2(Bx)$	$\cosh(2B)$	$1+4B^2$
$\varphi_{in}=\pi/2$ (phase noise)	$\cosh^2(Bx)+\frac{\kappa^4}{4B^2x^2}\sinh^2(Bx)$	$\cosh(2B)$	1
$\varphi_{in}=\varphi_{max}$ K_{max}	(38)	$\exp(2B)$	$\left(B+\sqrt{B^2+1}\right)^2$
$\varphi_{in}=\varphi_{min}$ K_{min}	(38)	$\exp(-2B)$	$\left(B-\sqrt{B^2+1}\right)^2$
Averaging over φ_{in} K_{av}	$1+\frac{2}{x^2}\sinh^2(Bx)$	$\cosh(2B)$	$1+2B^2$

output of the medium:

$$K=(u_{12}^2+u_{22}^2)\sin^2\varphi_{in}+(u_{11}^2+u_{21}^2)\cos^2\varphi_{in}+(u_{11}u_{12}+u_{21}u_{22})\sin(2\varphi_{in}), \quad (34)$$

$$\varphi_{out}=\arctan\frac{u_{21}+u_{22}\tan\varphi_{in}}{u_{11}+u_{12}\tan\varphi_{in}}. \quad (35)$$

Therefore, the noise gain coefficient K and the output noise phase φ_{out} are defined by three quantities: the B-integral, transverse noise wavenumber κ, and noise phase φ_{in} at the input of the medium. Note that φ_{in} is completely determined by the noise, while the B-integral, on the contrary, is independent of the noise and is defined by the nonlinear medium (n_2) and the plane wave intensity I. The dimensionless noise wavenumber κ (28) is defined by the noise ($k_\perp$) as well as by the nonlinear medium length L, which depends on the product In_2 for a given B-integral. This important circumstance permits controlling SSSF for a given value of B (see Section 4.3).

An analysis of expression (34) suggests that the noise gain coefficient K essentially depends on φ_{in} and for certain values of φ_{in} may be smaller than unity, even in the instability domain (27). The noise phase is usually a random quantity evenly distributed in the interval from 0 to 2π, but prior to averaging expression (34) over φ_{in}, let us make two important remarks.

First, there are two singled-out values of φ_{in}: $\varphi_{in}=0$, which corresponds to the amplitude noise, and $\varphi_{in}=\pi/2$, which corresponds to the phase noise. In the propagation in a vacuum to the nonlinear element, the amplitude noise rapidly transforms to the phase one and vice versa, with the result that φ_{in} may be treated as a random quantity. Sometimes the surface of the nonlinear element itself is an important noise source. In this case, the deviation of the surface from a perfectly plane surface gives rise to phase noise, while the existence of dust particles, scratches, etc. gives rise to the amplitude noise.

Second, for every κ there exists a value $\varphi_{in}=\varphi_{max}$ ($\varphi_{in}=\varphi_{min}$), whereby the gain coefficient assumes its maximal (minimal) value K_{max} (K_{min}):

$$\varphi_{max}=-\frac{\pi}{4}-\frac{1}{2}\arctan\left(\frac{\kappa^2-2B}{2Bx}\tan(Bx)\right)+\pi N, \quad (36)$$

where N is an integer,

$$\varphi_{min}=\varphi_{max}-\frac{\pi}{2}, \quad (37)$$

with

$$K_{max}=K_{av}+\sqrt{K_{av}^2-1}, \quad K_{min}=K_{av}-\sqrt{K_{av}^2-1}=\frac{1}{K_{max}}, \quad (38)$$

$$K_{av}(B,\kappa)=1+\frac{2}{x^2}\sinh^2(Bx), \quad (39)$$

where K_{av} is the gain coefficient (34) averaged over the evenly distributed random phase φ_{in}. We note that for $B\gg 1$ the average noise gain coefficient K_{av} is equal to precisely half the maximal one. Considering that $x(\kappa=0)=x(\kappa=\kappa_{cr})=0$ and $x(\kappa=\kappa_{max})=1$, it is easy to obtain simple expressions for the gain for noise propagating at small angles ($\theta\ll\theta_{cr}$) and at the most dangerous angles ($\theta=\theta_{max}$). As one can see from Table 2, for $\theta\ll\theta_{cr}$, the phase noise is not amplified at all, and the amplitude one, on the contrary, undergoes high amplification.

In some cases, it is possible to control the noise phase, which permits suppressing SSSF. However, in most cases, φ_{in} is a random quantity, and in the subsequent analysis we will use the averaged gain coefficient K_{av} (39). Since $K_{av}(B,\kappa)$ significantly depends on wavenumber κ (Fig. 13a), throughout the instability band (27) the noise gain $G(B)$ depends of the spectral noise power density $S_n(z=0,\kappa)$ at the input of the nonlinear element:

$$G(B)=\frac{P_n(z=L)}{P_n(z=0)}=\frac{\int_0^\infty S_n(z=0,\kappa)K_{av}(B,\kappa)\kappa\,d\kappa}{\int_0^\infty S_n(z=0,\kappa)\kappa\,d\kappa}, \quad (40)$$

where P_n is the noise power. In practice, it is convenient to estimate P_n using the formulas obtained in Ref. [173], which relate P_n to the deviation of intensity from the average value I_{av}:

$$\mathrm{rms}=\left(1+\sqrt{\frac{P_n}{P}}\right)^2-1, \quad \frac{I_{peak}}{I_{av}}=\left(1+5\sqrt{\frac{P_n}{P}}\right)^2, \quad (41)$$

where rms is the root-mean-square deviation normalized to I_{av}, I_{peak} is the peak intensity, and P is the beam power.

SSSF was traditionally studied in nanosecond laser beams, whose typical intensity amounted to several GW cm^{-2}. Putting for an estimate $n_2=3\times10^{-16}$ cm^2 W^{-1} and $I=2.5$ GW cm^{-2}, from formula (30) we obtain the most dangerous angle $\theta_{max}\approx 1$ mrad and the corresponding spatial scale $\Lambda_{max}=\lambda/\theta_{max}\approx 1$ mm. Since the main noise sources (dust particles, scratches, roughness) are significantly smaller

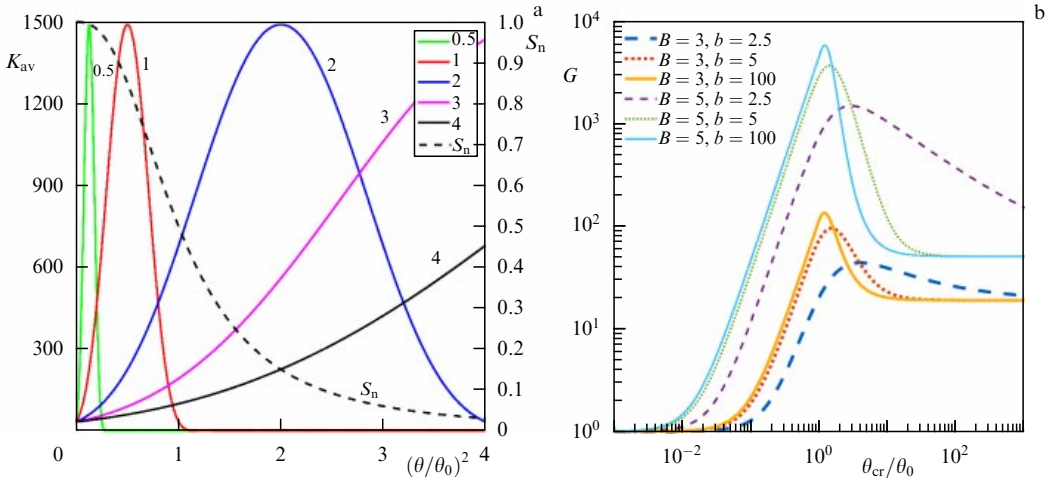

Figure 13. (Color online.) (a) Angular spectra S_n (43) of the noise at the input of the nonlinear element for $b = 5$ and of the noise gain K_{av} (39) for $B = 4$ and $\theta_{cr}/\theta_0 = 0.5, 1, 2, 3$, and 4. (b) Dependence of integral noise gain G (44) on θ_{cr}/θ_0 for $B = 3$ (thick curves) and $B = 5$ (thin curves) for $b = 2.5$ (dashed curves), $b = 5$ (dotted curves), and $b = 100$ (solid curves).

in size, it was commonly assumed in [168, 173, 174] that the noise has a uniform spectrum for $\theta < \theta_0$ throughout the instability band $0 < \theta < \theta_{cr} = \sqrt{2}\theta_{max}$. Assuming $S_n = \text{const}$ for $\theta < \theta_0$ and $S_n = 0$ for $\theta > \theta_0$, from expression (40) we obtain

$$G\left(B, \frac{\theta_0}{\theta_{cr}}\right) = \left(\frac{\theta_{cr}}{\theta_0}\right)^2 \int_0^{(\theta_0/\theta_{cr})^2} K_{av}(B, \xi)\, d\xi\,. \qquad (42)$$

Attempts of analytical integration in expression (42) using Eqn (39) do not meet with success. However, for $\theta_0 = \theta_{cr}$, it was possible to obtain an approximate expression $G(B) \approx \cosh(1.83B)$ [174]. For ultrahigh-power femtosecond lasers, the assumption of a uniform noise spectrum is less founded, which is thoroughly discussed in Section 4.2.

4.2 Special feature of small-scale self-focusing in ultrahigh-power lasers: a large critical angle

A fundamentally important distinction between SSSF in ultrahigh-power femtosecond lasers and nanosecond lasers is significant broadening of the instability range due to an increase in angle θ_{cr}. This is because the breakdown threshold of optical elements in the femtosecond range is much higher, and the laser radiation intensity amounts to several TW cm^{-2} rather than several GW cm^{-2}. The most dangerous angle θ_{max} is proportional to the square root of the intensity and is therefore 30 times larger. Putting for an estimate $n_2 = 3 \times 10^{-16}$ cm^2 W^{-1} and $I = 2.5$ TW cm^{-2}, from formula (30) we obtain $\theta_{max} \approx 30$ mrad and the corresponding spatial scale $\Lambda_{max} = \lambda/\theta_{max} \approx 30$ μm.

For these large angles, the assumption that the noise spectrum is uniform throughout the instability band, $0 < \theta < \theta_{cr} = \sqrt{2}\theta_{max}$, is nonphysical. Evidently the spectral noise power density decreases for large angles. The spectral shape and the law of decrease are fundamentally different from those for the amplitude and phase noises.

The cause of amplitude noise lies with optical defects, which are responsible for zero intensity at some points in the cross section of the beam: dust particles and scratches. The amplitude noise spectrum caused by particles is defined by the noise spectrum of one particle — the Bessel function — and the distribution of dust particles over their diameter Λ_{dust} [175]. For a small angle, $\theta \ll \lambda/\Lambda_{dust}$, the noise has a uniform spectrum.

The cause of phase noise is the wavefront distortions introduced by optical elements. The nonuniformity of the refractive index is usually a large-scale one and does not make significant contributions to the noise at high spatial frequencies, while the surface profile of optical elements, by contrast, contains the entire spectrum. The spectral noise density is defined by the spectral density of the surface profile, which may be approximated by a power law at high frequencies [175, 176].

Note that the small-scale noise rapidly transforms to phase noise from the amplitude one, i.e., φ_{in} is a random quantity for both the amplitude noise and the phase ('by origin') one. However, the modulus of the spectrum remains invariable during propagation, and so S_n is the superposition of the amplitude and phase noise spectra. This issue calls for a special investigation. Here, we restrict ourselves, following Ref. [177], to a consideration of SSSF for a model spectrum:

$$S_n(z = 0, \theta) = \frac{S_0}{1 + (\theta/\theta_0)^b}\,, \qquad (43)$$

which is independent of θ for $\theta \ll \theta_0$ and decreases for large θ according to the power law $1/\theta^b$. This spectrum makes possible a qualitative description of SSSF in ultrahigh-power femtosecond lasers, as well as of the methods for its suppression. For $b \to \infty$, formula (43) describes a uniform distribution in the interval $0 < \theta < \theta_0$. We perform integration in the expression (40), using formulas (39) and (43), to obtain

$$G\left(B, b, \frac{\theta_0}{\theta_{cr}}\right) = \frac{1}{J}\left(\frac{\theta_0}{\theta_{cr}}\right)^{b-2} \int_0^{\infty} \frac{K_{av}(B, \xi)}{(\theta_0/\theta_{cr})^b + \xi^{b/2}}\, d\xi\,, \qquad (44)$$

where $J = \int_0^{\infty} d\xi/(1 + \xi^{b/2})$. For $b \leqslant 2$, the integral in expression (44) diverges at infinity and the upper limit should be replaced with a finite value. For $\theta_{cr} \to 0$, the gain $G \to 1$, since the noise fraction which falls into the amplification band tends to zero (Fig. 13a). For $b \to \infty$ and $\theta_{cr} < \theta_0$, expression (44) passes into expression (42), so that the gain G is described

well by the approximation

$$G(B) \simeq 1 + \left(\frac{\theta_{cr}}{\theta_0}\right)^2 \sinh(1.84B)\,. \qquad (45)$$

As is clear from formula (45), the quantity $G-1$ rises proportionally to θ_{cr}^2. This is explained by the fact that the instability band is proportional to θ_{cr} and integration 'over the area' gives a factor θ_{cr}^2. For $\theta_{cr} > \theta_0$, the growth of function $G(\theta_{cr})$ slows down (Fig. 13b). The reason is as follows: although the instability band broadens, its right edge enters the angular domain $\theta > \theta_0$, where there is no noise, and, accordingly, this domain does not make a contribution to the gain (Fig. 13a). On a further increase in θ_{cr}, the growth of function $G(\theta_{cr})$ is replaced with its decrease, and for $\theta_{cr} = 2^{1/2}\theta_0$ the gain G lowers to a value $G(\theta_{cr} = \theta_0)$, since the twofold broadening of the instability band is exactly compensated by the fact that only half of this band falls in the domain where there is noise. Finally, for $\theta_{cr} \gg \theta_0$, only the left edge of the instability band enters the angular domain $\theta < \theta_0$, and function G tends to $1 + 2B^2$ — the gain for low spatial frequencies (see Table 2). We note that $G(\theta_{cr} \gg \theta_0)$ is much lower than $G(\theta_{cr} \approx \theta_0)$.

In a more realistic situation, $2.5 < b < 5$, for $\theta_{cr} < \theta_0$, the situation is qualitatively the same, which is clearly demonstrated by Fig. 13b. For $\theta_{cr} > \theta_0$, the law of decrease of function $G(\theta_{cr})$ essentially depends on the law of decrease of the spectral noise density (43). However, in the limit $\theta_{cr} \gg \theta_0$, G tends to $1 + 2B^2$. Therefore, for $b > 2$, a significant increase in θ_{cr} in going from nanosecond lasers to femtosecond ones (see above) results in a lowering of G and the consequential increase in the maximum admissible B-integral values. To state it in different terms, the traditional limitation $B < 2-3$ for nanosecond lasers is relaxed for high-power femtosecond lasers owing to a significant increase in θ_{cr}. A quantitative determination of this relaxation invites detailed investigations of the angular noise spectrum in a broad angular range up to 0.1 rad.

For the subsequent discussion, we do well to note that the main contribution to integral (44) for large values of the B-integral ($B > 5$) is made by the range $\xi \approx 0.5$, i.e., $\theta \approx \theta_{max}$. To diminish G, it is therefore necessary to cleanse the beam of noise in the most dangerous angular domain θ_{max}. Since the characteristic value of θ_{max} is quite high — several dozen mrad — to suppress SSSF, use can be made of beam self-filtering during the propagation in free space over quite a short distance, which is the concern of Section 4.3.

4.3 Suppression of small-scale self-focusing by beam self-filtering

Mironov et al. [86] proposed an original method for beam cleansing for suppressing SSSF (Fig. 14). When an optical element is located away from the source noise, the most 'dangerous' noise components (with θ of the order of θ_{max}) escape from the beam aperture. In this case, the free space itself becomes a spatial filter. The main sources of noise are the surfaces of mirrors or diffraction gratings. By accommodating an optical element at a sufficiently long distance L_f from the last mirror or grating, it is possible to sideline the 'dangerous' noise components from the domain of interaction with the strong wave. This takes place for small viewing angles θ_v:

$$\theta_v = \frac{\Theta_v}{n_0} = \frac{1}{2n_0}\frac{d}{L_f}\,, \qquad (46)$$

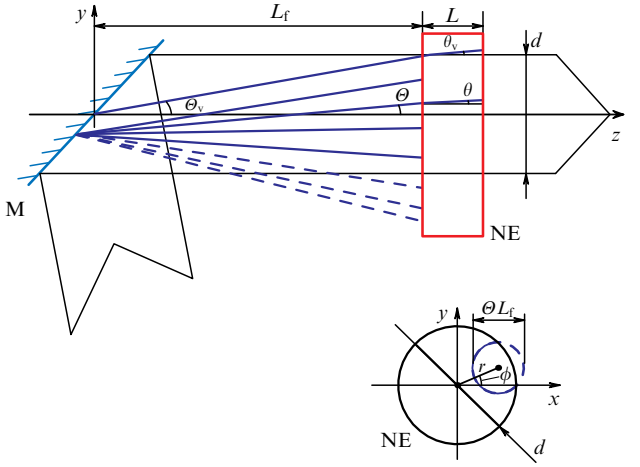

Figure 14. (Color online.) Beam self-filtering in propagation in free space: part of the noise (shown with dashed lines) escapes from the beam aperture in the propagation away from the source noise (mirror M) to a nonlinear element (NE).

where d is the beam diameter. Here, as above, interior angles (inside the nonlinear element) are denoted by lowercase letters (θ_v) and exterior angles by capital ones (Θ_v). The spatial noise present in the beam prior to reflection from the last mirror is also filtered out, because its distance from the nonlinear element is even longer and θ_v is even smaller. As is clear from formula (30), the magnitude of θ_{max} is proportional to the square root of the radiation intensity and is independent of the B-integral. For nanosecond lasers, the characteristic radiation intensity is of the order of several GW cm^{-2}, which yields θ_{max} of about 1 mrad and makes the self-filtering in free space hardy possible, because L_f is too large. For femtosecond lasers, the intensity is ~ 1 TW cm^{-2} and angle θ_{max} is significantly larger — several dozen mrad — which results in reasonable distances L_f even for large diameters d. Note that in millijoule-level lasers d is quite small and self-filtering is realized for very short L_f, one might say 'automatically' (see, e.g., Refs [35, 67, 71, 178]).

The self-filtering of high-intensity radiation was borne out in Refs [86, 179] with a qualitative experiment, in which the degree of glass damage under SSSF was investigated in relation to L_f. As demonstrated experimentally in Ref. [86], under frequency doubling in a potassium dihydrogen phosphate (KDP) crystal for $I = 5$ TW cm^{-2} and $B = 6$, the filamentation and breakdown of the crystal were observed for a viewing angle $\Theta_v = 40$ mrad and were completely absent for $\Theta_v = 10$ mrad. In Ref. [179], the degradation of a 4-mm-thick glass plate was measured upon irradiation of one spot by 100 pulses. Three kinds of damage were observed: catastrophic (high brightness of color centers in the beam area); small turbidity of the plate; and the absence of any damage. The effect of self-filtering for small angles θ_v is clearly seen in Fig. 15, in which experimental points are plotted in the (B, θ_v) parameter plane.

The results of measurements of the gain factor $K(\theta)$ of the spatial noise spectrum are presented in relation to the distance L_f from the noise source in Ref. [169]. The measurements were made by two independent methods: direct [174, 180] and indirect [180]. The beam passed through a slightly matted thin (0.2 mm) glass plate, which introduced amplitude noise. The nonlinear element was a 10-mm-thick glass plate. The beam

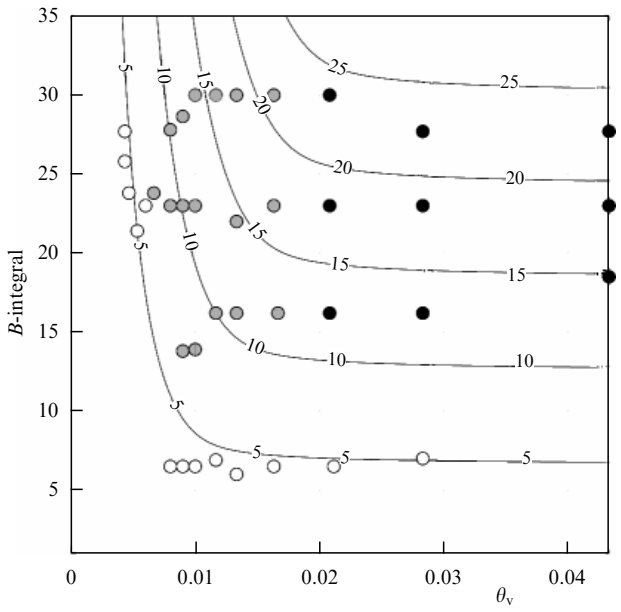

Figure 15. Experimental data from Ref. [179] showing the lowering of plate transmittance due to turbidity: significant (black circles), slight (grey circles), and zero (empty circles). The curves show the theoretical levels of the quantity lg G calculated using expression (49).

energy was equal to 0.5 mJ, the pulse duration to 70 fs, $\theta_{max} = 5.2$ mrad, $B = 1.4$.

For direct gain measurements, as in Refs [165, 174, 180], the radiation was focused with a spherical mirror, and accommodated in its focal plane was a plane mirror with an opening for rejecting the principal (non-noise) beam. The opening diameter was large enough to transmit the whole principal beam, including its wings, and so only the noise radiation was reflected from the mirror. Recorded in this way was the angular noise spectrum with the small-angle domain 'cut out.' The noise gain $K(\theta)$ was calculated using normalization. In the indirect measurement of $K(\theta)$, after the nonlinear element, the beam was delivered to a lens, which imaged the output plane of the noise source to a CCD camera (CCD: charge coupled device). In Ref. [180], it was shown that these measurements permit calculating $K(\theta)$. The distance L_f between the nonlinear element and the noise source varied from 12 to 600 mm. Both methods revealed quantitative agreement between experimental and theoretical data. They also confirmed that the angular spectrum domain in which amplification occurs decreases with increasing L_f and that self-focusing practically vanishes on a further increase in L_f. Numerical simulations of the propagation of a noisy beam in a nonlinear medium [169] performed using the program 'Fresnel' [173] also confirmed the effect of suppression of self-focusing.

Free space is therefore a spatial frequency filter, whose transmittance $T_f(\kappa, \theta_v)$ depends on the viewing angle θ_v. The efficiency of this filter may be estimated by including it in expression (40):

$$G = \frac{P_n(z = L)}{P_n(z = 0)} = \frac{\int_0^\infty T_f(\kappa, \theta_v) S_n(z = 0, \kappa) K_{av}(B, \kappa) \kappa \, d\kappa}{\int_0^\infty S_n(z = 0, \kappa) \kappa \, d\kappa} . \quad (47)$$

Ginzburg et al. [177] made the following estimate of function $T_f(\kappa, \theta_v)$, proceeding from geometrical optics. Let 'noise' rays emanate at an angle θ to the z-axis from each point (r, φ) of the beam cross section in the noise source plane. In the plane of the nonlinear element, a fraction of these rays will find themselves in the beam aperture (shown with solid lines in Fig. 14) and a fraction will be beyond the aperture (shown with dashed lines in Fig. 14). The fraction $t_f(\kappa, \theta_v)$ of rays that find themselves in the aperture is the transmittance of the noise emanating from point (r, φ). Integrating $t_f(\kappa, \theta_v)$ over the cross section gives the expression for T_f:

$$T_f\left(\frac{\theta}{\theta_v}\right) = \frac{1}{\pi} \int_0^1 \arccos\left[\frac{(\theta/\theta_v)^2 + y - 1}{2\sqrt{y}\,\theta/\theta_v}\right] dy . \quad (48)$$

If the expression in square brackets is greater than 1(smaller than -1), the arccosine must be replaced with zero (unity). As would be expected, T_f depends only on the ratio θ/θ_v. By substituting expression (48) into expression (47), it is possible to generalize expression (44) for the noise gain.

The self-filtering effect is clearly demonstrated in Fig. 16a, which shows that the noise power for $\theta_{cr} > \theta_v$ becomes significantly lower in the domain of highest gain, i.e., for $\theta \approx \theta_{max} = \theta_{cr}/2^{1/2}$. For $\theta_{cr} > 4\theta_v$, practically all unrejected

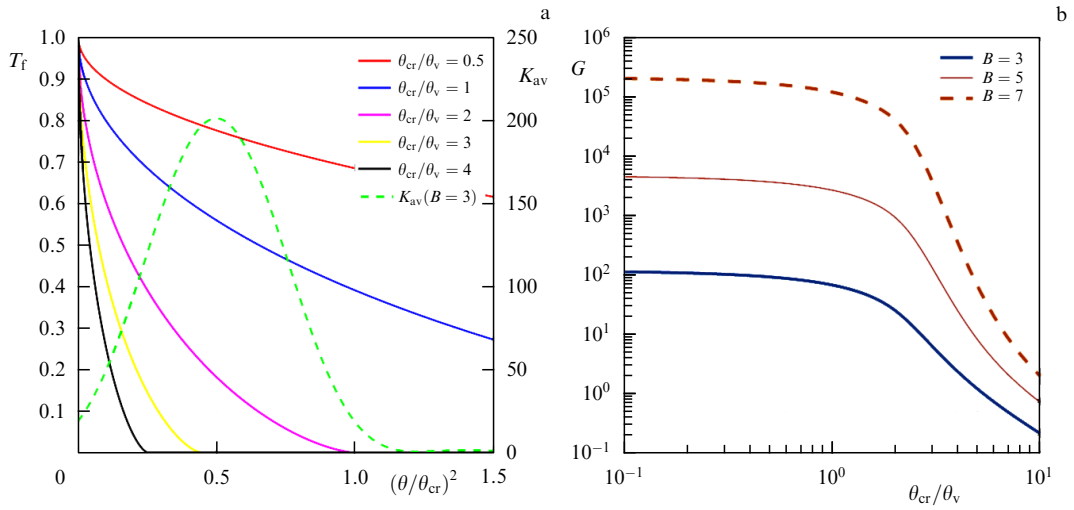

Figure 16. (Color online.) (a) Angular spectra of free-space transmittance T_f (48) for different $\theta_{cr}/\theta_v = 0.5$, 1, 2, 3, and 4 (solid curves) and noise gain factor K_{av} (39) for $B = 3$ (dashed curve). (b) Dependence of integral noise gain G (49) on θ_{cr}/θ_v for a uniform noise spectrum in the angular range $0 < \theta < 2\theta_v$ and $B = 3$ (bold curve), $B = 5$ (thin curve), and $B = 7$ (dashed curve).

noise has a gain factor close to $K_{av}(\theta = 0) = 1 + 2B^2$, which is much lower than $K_{av}(\theta = \theta_{max}) = \cosh(2B)$ (see Table 2). Quantitatively, the self-filtering effect depends on the input noise spectrum, i.e., on parameters b and θ_0. When the noise spectrum S_n prior to filtering is uniform in the domain $0 < \theta < \theta_{cr}$ and $S_n = 0$ for $\theta > \theta_{cr}$, from expressions (47) and (48), in view of formula (39) we obtain

$$G\left(B, \frac{\theta_{cr}}{\theta_v}\right) = \int_0^1 T_f\left(\frac{\theta_{cr}}{\theta_v}\sqrt{\xi}\right) K_{av}(B, \xi)\, d\xi\,. \qquad (49)$$

Figure 16b shows the dependence $G(\theta_{cr}/\theta_v)$ plotted using expression (49) for different B. As is clear from the figure, G shows a significant decrease for $\theta_{cr} > 2\theta_v$. In particular, $G(B = 7, \theta_{cr} = 5\theta_v) = G(B = 3, \theta_{cr} \ll \theta_v)$. Therefore, a large value of θ_{cr} suppresses SSSF: the spectral noise density decreases for large angles (see Section 4.2) and beam self-filtering (if $\theta_{cr} > \theta_v$) occurs in the free-space propagation. The simultaneous action of these two effects is discussed in Ref. [177].

4.4 Suppression of small-scale self-focusing by nonlinear dispersion

SSSF development in a medium with inertialess nonlinearity was investigated in Refs [109, 110] for few-cycle laser pulses, i.e., with the inclusion of the last terms in Eqn (4) responsible for nonlinear dispersion — the intensity dependence of the group velocity (5). It was analytically shown that a uniform solution remains unstable, but the type of instability changes — it becomes convective. The result is that SSSF would be suppressed for pulses shorter than some duration, which was confirmed numerically. Physically, this is attributable to the fact that intensity perturbations, which have a lower group velocity, lag behind and shift to the trailing pulse edge, where the intensity is significantly lower and their growth slows down. An estimate of the pulse duration, whereby the growing perturbations stabilize due to their displacement to the trailing edge of the pulse, yielded a figure of about 10 laser field cycles.

Therefore, for a pulse duration of 25 fs and shorter, an additional SSSF suppression mechanism appears, which does not call for any special effort or devices. So far, the effect of SSSF suppression due to nonlinear dispersion has not been experimentally demonstrated.

4.5 Application of traditional small-scale self-focusing suppression methods in ultrahigh-power lasers

Beginning in the 1970s, SSSF suppression methods were vigorously developed in connection with the advancement of neodymium glass lasers, whose output energy is limited, as a rule, by precisely the SSSF. The direct method of SSSF suppression consisted in the use of low-n_2 glasses, for instance beryllium-fluoride glasses [181]. Use is also made of circular polarization, for which the effective value of n_2 is 1.5 times smaller than for the linear one, both in isotropic media [155, 168, 182, 183] and in ceramics [184]. As shown in Refs [165, 167], by selecting the orientation of a cubic crystal, it is also possible to lower the effective value of n_2. The population trapping in the propagation of two waves whose frequencies differ by the Raman shift also results in a lowering of n_2 [185]. These methods are basically unsuited for CafCA, because a large value of the B-integral is required for efficient compression, and low values of n_2 have to be compensated by a large thickness of the nonlinear element (3).

Unsuitable for CafCA in ultrahigh-power lasers are diverging beams, whose diameter varies significantly in the propagation in a nonlinear element [186–188], as well as beam decoherentization [189–191] and the simultaneous propagation of several beams in one nonlinear element [192, 193]. SSSF may be completely suppressed by repeaters, which was shown theoretically [151–153, 155] and experimentally [151]. These studies pertain to nanosecond lasers. The use of repeaters for CafCA with picosecond lasers was theoretically considered in Refs [93, 194]. In this case, the main problem is the shortening of the repeater length, which, according to Ref. [93], is of the order of 10 cm, even for a nonlinear element thickness of several centimeters, which is hard to realize in practice. An even greater shortening in moving to ultrahigh-power femtosecond lasers is impossible.

The fragmentation of a nonlinear element — breaking it into several parts without repeaters between them — also presents difficulties, since the elements become even thinner. However, this limitation is removed if use is made of thin polymer films, which is discussed in detail in Section 5.4. In Sections 4.5.1 and 4.5.2, we will consider methods for SSSF suppression, which may be applied for CafCA in the future: the use of spatial filters and media with $n_2 < 0$.

4.5.1 Spatial filters. The use of a spatial filter is the most widespread and efficient method of SSSF suppression in nanosecond lasers. The spatial filter consists of a pair of confocal lenses (Keplerian telescope) with an aperture stop located in the focal plane (see image *2* in Fig. 17). The intensity distribution at the focus is the spatial (angular) spectrum of a beam, and high spatial frequencies are therefore absorbed by the aperture stop. The largest angle Θ_{sf} that passes through the aperture is defined by its radius r_{sf} and the focal length f_{sf} of the lens:

$$\Theta_{sf} = \frac{r_{sf}}{f_{sf}}\,.$$

Therefore, the smaller Θ_{sf}, the weaker the noise that passes through the filter. The minimal aperture size is limited for two reasons. The first is that the plasma generated at the aperture stop must not have time to screen the beam, i.e., the time of its flight to the axis should be longer than the beam duration. The second one is that the beam must freely pass through the aperture, since the diffraction of even very 'distant' wings by the aperture will give rise to new spatial noise. In other words,

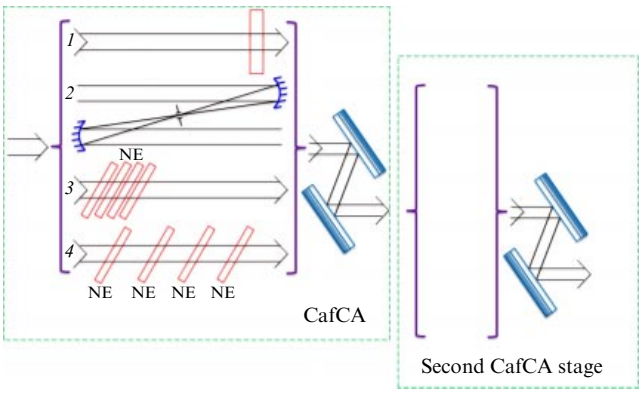

Figure 17. (Color online.) CafCA with various methods of SSSF suppression: *1* — self-filtering in free-space propagation; *2* — spatial filters; *3* — nonlinear element fragmentation; *4* — nonlinear element fragmentation with self-filtering.

the magnitude of Θ_f should be much greater than the diffraction limit Θ_{dif}.

Spatial filters were first employed for SSSF suppression at the Lawrence Livermore National Laboratory [195–197]. In these papers, it was shown, in particular, that Θ_f must be 10–20 times greater than Θ_{dif}. More recently, in Refs [186, 198, 199], the efficiency of SSSF suppression with the use of spatial filters, which are now used in almost all high-power nanosecond lasers [200, 201], was experimentally borne out. A theoretical analysis of the operation of spatial filters may be found in Refs [173, 202, 203], and the practical aspects of their use in Refs [204, 205].

The use of spatial filters for CafCA was discussed in Refs [20, 72, 88]. It was pointed out that N nonlinear elements separated by spatial filters make it possible to obtain spectral broadening corresponding to the B-integral equal to NB_1 and avoid SSSF, provided the B-integral in each element $B_1 < 3$. A detailed numerical investigation of the CafCA for picosecond pulses with the number of stages up to $N = 10$ for $B_1 = 1.4$ was performed in Ref. [194]. The simulation data suggest that the SSSF-induced beam distortions remain acceptable for $N = 5$, and even for $N = 10$. In Ref. [87], numerical simulations were made of the propagation of a 120-femtosecond 13-PW power pulse through nine nonlinear elements with $B_1 = 5.3$ separated by eight spatial filters. The simulations suggested the feasibility of pulse compression to 4–5 fs without significant degradation of beam quality. In the numerical simulation [20], a 27-fs-long pulse was initially compressed to 6.4 fs ($B = 6.1$) and then, after a spatial filter, compressed to 2.1 fs ($B = 4.4$).

Theoretical simulations show the promise of using spatial filters for CafCA, but their practical application is fraught with several problems. Since it is impossible to employ lenses, use has to be made of spherical mirrors. To minimize the inevitably introduced astigmatism, the mirrors should have a small numerical aperture, making the telescopes quite cumbersome. The use of off-axis parabolas shows more promise. Another drawback is that the stop and the output mirror of the telescope are themselves sources of noise, which is not filtered out. Herein lies a difference from beam filtering in propagation in free space (see Section 4.3), where no mirrors are required. From this viewpoint it would be instructive to place the nonlinear element between the stop and the output mirror of the spatial filter. This geometry offers additional advantages related to the possibility of varying the beam intensity in the nonlinear element.

It is significant that beam cleansing in the spatial filters of ultrahigh-power lasers is their important advantage over nanosecond lasers, in which the ratio $\Theta_{max}/\Theta_{dif}$ is not very large, and therefore the condition $\Theta_{dif} \ll \Theta_f \ll \Theta_{max}$ is not always easy to fulfill. As indicated above, for ultrahigh-power lasers, the magnitude of Θ_{max} is considerably larger, which significantly simplifies the fulfillment of this condition and makes beam cleansing more efficient. It is possible to estimate the efficiency of this cleansing by assuming that the noise spectrum becomes uniform ($b = \infty$) inside the angle $\theta_0 = \theta_f$ on passing through the filter. Then, as is clear from Fig. 13b (the curves for $b = 100$), on the condition that $\theta_{cr} > 10\theta_f = 10\theta_0$, which is always fulfilled, the noise gain $K_{av} = 1 + 2B^2$. The noise power at the output of the nonlinear element is proportional to $(1 + 2B^2)\theta_f^2$.

Therefore, the use of spatial filters for CafCA is an intricate experimental task which may, nevertheless, be realized in the future.

4.5.2 Media with negative n_2. As a rule, in the visible and near-infrared ranges, $n_2 > 0$, which results in self-focusing. There are, however, exceptions to this rule: media with negative n_2, in which the radiation experiences defocusing (self-defocusing). By way of example, mention can be made of cesium vapor (for a wavelength of 1060 nm) [206], xenon (for a wavelength of 248 nm) [207], GaAs (for a wavelength of 1060 nm) [208], AlGaAs (for a wavelength of 850 nm) [209], and other semiconductors [210, 211]. These media are used compensate (subtract) the nonlinear phase incursion which inevitably appears in laser amplifiers. These media are not quite suited for CafCA: gaseous media necessitate windows, in which $n_2 > 0$, and semiconductors cannot withstand so high an intensity. Furthermore, in both cases, the band is much shorter than required for femtosecond pulses. Measurements of the cubic nonlinearity tensor χ in a beta-barium borate (BBO) crystal [212] showed that $\chi_{eeee} < 0$ (e is an extraordinary wave), but this statement calls for verification, since the measurement uncertainty exceeded $|\chi_{eeee}|$. Furthermore, the BBO crystal apertures are small, which limits the possibility of their use for CafCA.

Recently papers have appeared which state that organic doping of KDP crystals results in a positive-to-negative n_2 sign change. The measurements were made for crystals doped with formic acid (0.5 mol.% and 1 mol.%) [213] and with citric acid (1 weight%) [214]. The absolute value $|n_2|$ in the doped crystals turned out to be much smaller than n_2 for non-doped KDP, which hampers its use for CafCA. A similar result (change of n_2 sign) was obtained by the same group [215] for KDOP (potassium dihydrogen orthophosphate) crystals doped with tartaric acid. In this case, the absolute value $|n_2|$ was approximately the same, and extremely large at that. It is pertinent to note that the authors of these papers specify neither the orientations of the KDP and KDOP crystals nor the radiation polarization with which the measurements were made. Without these data, the results of measurements are hard to interpret. At the same time, if attempts to obtain a doped KDP crystal with a negative n_2 meet with success, this would be a panacea for SSSF, since the KDP crystals presently grown measure 40 cm or more. We note that the cubic nonlinearity measurements for deuterated KDP (DKDP) crystals made in Refs [216, 217] showed a strong dependence of n_2 on the degree of deuteration, but the sign of n_2 was always positive.

Another way to obtain a medium with a negative n_2 is to use the effect of cascade second harmonic generation discovered in Ref. [218]: when deviating from the phase matching direction in the course of frequency doubling, an addition to the refractive index appears, which depends linearly on the intensity, i.e., an effective cubic nonlinearity and an addition to the nonlinear refractive index n_2^{casc} appear (see, e.g., Refs [219–222]). The sign of n_2^{casc} is determined by the sign of detuning of the wavevectors of the interacting waves of the first and second harmonics, which permits obtaining $n_2^{casc} < 0$. Physically, n_2^{casc} is explained by the fact that an energy transfer occurs from the first harmonic to the second and vice versa in the case of deviation from the phase matching direction. The energy efficiency of this transfer is low for large detuning — practically all energy remains in the first harmonic — but an additional shift appears in the phase of the first harmonic wave, since the phase velocities of the first and second harmonic waves are different. The effect is absent ($n_2^{casc} = 0$) for exact matching, since the phase velocities of the harmonics are equal, as well as away from

the matching, since there is no energy transfer to the second harmonic. The sign of the effective nonlinear refractive index depends on the balance between the contributions of Kerr nonlinearity and cascade generation: $n_2^{\text{eff}} = n_2 + n_2^{\text{casc}}$.

One of the crystals in which $n_2^{\text{eff}} < 0$ is BBO. BBO crystals are employed to compensate a nonlinear phase shift [223–225], as well as to compress pulses without SSSF-related limitations. In Ref. [226], a 190-fs-long pulse was sequentially compressed in three BBO crystal stages to 97, 50, and 30 fs, respectively, and in Ref. [227] from 120 to 30 fs in one stage. In Ref. [228], a pulse with $\lambda_0 = 1.3$ μm was compressed in duration to several field cycles directly in a lithium niobate crystal. However, all these experiments were restricted to a low pulse energy and power. Scaling is limited primarily by the absence of wide-aperture crystals with a negative n_2^{eff}. According to numerical simulation data [79], self-compression is possible in KDP crystals and, consequently, n_2^{eff} may be negative, but we are unaware of its experimental confirmation to date. Among other disadvantages, mention should be made of the impairment of beam quality due to the walk-off of the extraordinary wave, the need to precisely align the crystal, and the wavelength dependence of n_2^{casc}.

5. Plastic: a new promising nonlinear material

As mentioned in the Introduction, a substantial limitation for CafCA at petawatt powers is the necessity of making a nonlinear element with a high aspect ratio d/L, since a high intensity requires a small thickness L and a high energy calls for a large diameter d. It is significant that the nonlinear element should not introduce significant wavefront distortions, which would impair the beam focusing on a target. The fabrication technology of traditional optical elements of glass and silica is developing evolutionally and is advancing to progressively higher aspect ratios. For instance, in Ref. [22] use was made of glass plates of thickness $L = 1$ mm and diameter $d = 20$ cm, which possessed a high optical quality. However, thinning to several hundred micrometers is an extremely intricate technological problem. An alternative was proposed in Ref. [22]: to use a thin 'plastic' film. The advantages of this approach are discussed in Sections 5.1–5.4.

5.1 Idea of using plastics

The word 'plastic' is hereinafter used for brevity and implies any amorphous thermoplastic polymer, for instance, polyvinylchloride (PVC), cellulose acetate, polyester, polyethylene terephthalate, or another one. The plastic must be transparent at the laser wavelength and strong, and have the same thickness throughout its aperture, ideally to within a fraction of the wavelength. Even the first testing in [94] of the plastic as a nonlinear element revealed that the phase distortion of the beam transmitted through 700-μm-thick polyethylene terephthalate used in everyday life amounted to half the wavelength for an aperture 20 cm in width. A higher-quality and thinner plastic introduces knowingly smaller distortions. Furthermore, measurements were made of radiation depolarization, which was equal to 0.02%, i.e., was negligible. Absorption was also negligible. Therefore, the linear optical properties of the plastic fully satisfy the requirements imposed by CafCA.

Plastics offer a number of advantages over glass and fused silica. The transverse 1-m dimension is standard, which is known to suffice not only for present-day lasers but also in the foreseeable future. The plastic production technology easily provides thicknesses of 100 μm or even less. Such thin films are made in rolls, permitting the use of a roller feed mechanism [81], which will feed the film in case it degrades. Considering the low cost of plastics, this may be done after each shot. With the use of thin films, it is convenient to specify the total thickness L by varying the number of layers. In Ref. [81], for instance, use was made of six layers of a 100-μm-thick film. Owing to the absence of limitations in transverse size, the plastic is accommodated at a Brewster angle, which practically rules out losses, even for a large number of layers.

Another advantage of plastics is the wide variety of materials, which gives hope for a diversity of properties, primarily of the nonlinear refractive index n_2 and group velocity dispersion k_2. Measurement data are hardly available for these parameters — this is the subject of investigation in the near future. In Sections 5.2–5.4, we discuss specific aspects in which the above advantages of plastics may be used for CafCA.

5.2 Increasing the critical angle of small-scale self-focusing

As mentioned in Section 4.2, a critically important feature of SSSF in ultrahigh-power femtosecond lasers is the significant increase in the critical angle θ_{cr} of SSSF. As shown in Section 4.2 (see also Fig. 13), the increase in θ_{cr} makes it possible to suppress the development of SSSF owing to the fact that the main noise does not fall into the highest gain domain as well as due to self-filtering of the laser beam (see Section 4.3 and Fig. 16). In other words, it is expedient to increase θ_{cr}. According to formula (30), this may be done using media with a large n_2. In polyethylene terephthalate, n_2 is approximately two times greater than in fused silica [94]. Measurements of n_2 for other plastics have not been carried out, but, considering the diversity of polymer materials that can be used as nonlinear elements, one would expect the appearance of plastics with even higher n_2.

Accommodating a nonlinear element at the Brewster angle also results in an increase in the critical angle, though not of the interior angle θ_{cr} but of the exterior Θ_{cr} one, as follows. In the case of normal incidence of a plane wave, evidently, $\Theta_{\text{cr}} = n_0\theta_{\text{cr}}$. However, when the incidence angle is equal to the Brewster angle, $\varphi_{\text{B}} = \arctan n_0$, and it is easily shown from Snell's law that

$$\Theta_{\text{cr}} = n_0^2\theta_{\text{cr}}\,, \tag{50}$$

i.e., the exterior-to-interior angle ratio is n_0 times greater than in the case of normal incidence. Important for SSSF suppression is not the increase in the absolute value of θ_{cr} but the increase in its ratio to the characteristic angle of spectral noise density θ_0 and to the viewing angle θ_{v} (see Figs 13 and 16). Since angles Θ_0 and Θ_{v} in a vacuum are independent of the angle of incidence on the nonlinear element, from formula (50) it follows that placing the nonlinear element at the Brewster angle will increase $\Theta_{\text{cr}}/\Theta_0$ and $\Theta_{\text{cr}}/\Theta_{\text{v}}$ by n_0 times in comparison with the corresponding figures at normal incidence. The interior angle ratios $\theta_{\text{cr}}/\theta_0$ and $\theta_{\text{cr}}/\theta_{\text{v}}$ will evidently increase by the same factor, since relation (50) for the exterior-interior angle ratio is valid for any indices: $\Theta_0 = n_0^2\theta_0$, $\Theta_{\text{v}} = n_0^2\theta_{\text{v}}$. Of course, a nonlinear element of glass or silica mounted at the Brewster angle will also increase Θ_{cr} by n_0 times, but a significant aperture widening is very problematic for these elements, while for plastic it is not. Note that media with a large n_2 usually possess

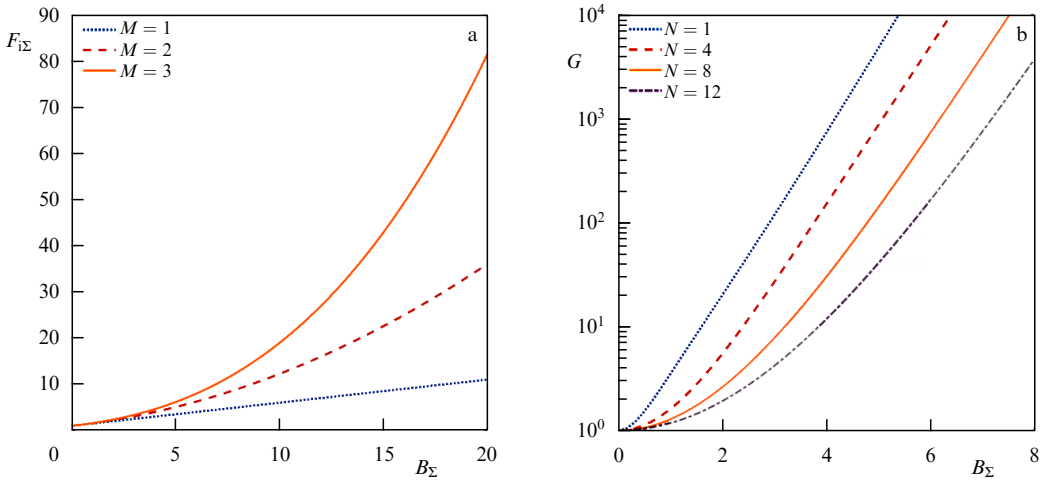

Figure 18. (Color online.) (a) Dependences of intensity enhancement factors on the total B-integral for a different number of stages M. (b) Dependence of gain G on B_Σ in the case of division of a nonlinear element into N similar fragments, in each of which the B-integral is equal to B_Σ/N.

a large n_0, and it is expedient to increase both refractive indices for increasing Θ_{cr}, Θ_{cr} being proportional to $n_2^{1/2}n_0^{3/2}$ (see Eqns (30) and (50)).

One of limitations on increasing the pulse intensity in the SPM in glass or silica is that a given value of the B-integral in accordance with formula (3) signifies the use of very thin elements. Plastic largely removes this limitation, which may be used for increasing the value of θ_{cr}, which is proportional to the square root of the intensity (30). This is especially significant for a two-stage compression.

5.3 Two-stage compression

The use of plastics opens the way to two- and multistage compression. By two-stage compression (two-stage CafCA) are meant two successive compressions: a nonlinear element, dispersive mirror(s), and another nonlinear element and more dispersive mirror(s) (see Fig. 17). This approach has been repeatedly used at the microjoule level [43, 69, 226]. However, in ultrahigh-power lasers it is necessary to employ very thin nonlinear elements, especially so in the second compression stage. We assume the same value of the B-integral in the two nonlinear elements, the second one being several-fold thinner than the first (by F_i times, where F_i is the intensity enhancement factor of the first stage). For ultrahigh-power lasers, this leads to a thickness of about 100 μm, which is possible only with the use of plastic. This is precisely why only the fragmentation of the nonlinear element, which increases the net B-integral, and a single compression were considered for glass or silica [87]. The idea of the two-stage compression of ultrahigh-power pulses was proposed by the authors of Ref. [20], who also proposed the use of plastics. The first, highly promising results were recently obtained [85].

Two-stage compression possesses a considerable advantage over nonlinear element fragmentation, with the result that the total B-integral B_Σ depends linearly on the number of stages M, while the net intensity enhancement factor $F_{i\Sigma}$ obeys a power law:

$$B_\Sigma = MB_1\,, \qquad F_{i\Sigma} = (1 + 0.49B_1)^M\,. \tag{51}$$

Here, for simplicity, we ignored dispersion and assumed equal B-integral values B_1 for all stages and therefore the same intensity enhancement factors F_i defined by formula (11c) for $D = 0$. All parasitic effects (SSSF, phase aberrations, lateral nonuniformity of compression) are defined by the total B-integral, B_Σ, irrespective of the number of compression stages. Figure 18a depicts dependence $F_{i\Sigma}(B_\Sigma)$ plotted using formulas (51) for one, two, and three compression stages. From the figure it is seen that for $B_\Sigma < 4$, one-stage compression ranks only slightly below the multi-stage one. However, for larger B_Σ, the increase in the number of stages to two and, all the more so, to three makes it possible to obtain significantly higher values of $F_{i\Sigma}$, i.e., a significantly higher pulse intensity. The second of expressions (51) and Fig. 18a are approximate, since they ignore dispersion and the fact that the pulse will not be Fourier-limited at the input of the second and subsequent nonlinear elements. To exactly include these two effects requires a more rigorous theory, described in Section 2. However, the corrections related to these effects are small (see Figs 4 and 9), and the accuracy of expressions (51) is quite sufficient for estimating $F_{i\Sigma}$.

A two-stage compression has three other advantages over the single-stage one, which permit fighting against SSSF more efficiently. The first is related to the fact that the pulse intensity in the second nonlinear element is much higher than in the first one. First, this increases the critical angle θ_{cr} and suppresses SSSF and, second, it has the effect that the values of θ_{cr} in the two nonlinear elements are different. Since the magnitude of θ_{cr} is proportional to the square root of In_2 (30), this difference may be further increased by using a plastic with a higher n_2 as the second nonlinear element. The noise enhancement factors will then have maxima at significantly different θ, which will lower the total noise enhancement factor. The second advantage is the possibility of beam cleansing (self-filtering or a spatial filter) between the stages. And, finally, the third advantage is that the pulse duration in the second nonlinear element is much shorter than in the first one. If this duration turns out to be no longer than 10 laser field cycles, SSSF in the second nonlinear element will be suppressed thanks to nonlinear dispersion (see Section 4.4).

5.4 Nonlinear element fragmentation

Fragmentation of a nonlinear element is the replacement of one element with N elements with the same total thickness without repeaters or spatial filters between them (see image *3* in Fig. 17). This is essentially different from multistage

compression, since dispersive mirrors are used only once. Unlike SSSF suppression by self-filtering and spatial filters, in this case, the SSSF suppression is implemented via phase effects rather than via the suppression of well-amplified spatial frequencies. The free propagation of light by a distance L_f reduces to noise phase incursion relative to a plane wave:

$$\varphi_f = \Theta^2 \frac{L_f}{\lambda} \pi . \quad (52)$$

By varying length L_f, it is possible to vary the noise phase at the input of the second nonlinear element, which will be the sum of the phase φ_{out} (35) at the output of the first element and phase φ_f (52). The noise gain (38) depends strongly on the input phase, and the gain may be smaller than unity. In optical systems comprising a periodic sequence of linear and nonlinear media, it is possible to suppress SSSF for many angles Θ, but not for all of them [152, 154, 186]. The use of nonequidistant geometry, whereby the thicknesses of nonlinear elements and the distances between them are different, is more efficient, which was observed experimentally in [229, 230] and explained theoretically in [229, 231]. Investigated in all these papers was the SSSF of nanosecond pulses. Future investigations will provide an answer to the question of how efficient the transfer of this idea to the realm of ultrahigh-power lasers is.

As indicated above, an important feature of CafCA for ultrahigh-power pulses is the large angles of maximum noise gain θ_{max} — several tens of milliradians. This permits using an amplitude effect apart from the phase one described in the forgoing. For such θ_{max} values, the free-space noise phase incursion φ_f ranges up to 2π at a distance L_f of about 1 mm. Therefore, for a 1-cm (or greater) spacing between the nonlinear elements, φ_f is a rapidly varying function of θ and, consequently, in the calculation of integral gain (in the integration over θ) the noise phase at the input of the second nonlinear element may be thought of as being random. Then, the phase effect described in the previous paragraph vanishes, but the amplitude effect persists: the net gain of N nonlinear elements is equal to the product of the gains in each of them. For N identical elements, the gain is equal to the gain of one element $K_{av}(B_1)$ taken to the power N. Proceeding from formula (39), it is readily shown that $K_{av}^N(B_1) \ll K_{av}(NB_1)$, i.e., nonlinear element fragmentation results in a significant lowering of the noise gain with retention of the total B-integral value $B_\Sigma = NB_1$. One can see from the formulas given in Table 2 that the fragmentation will lower the gain for $\theta = \theta_{max}$ by about a factor of 2^{N-1}.

According to Fig. 18b, which depicts the dependence of gain G on B_Σ calculated by formula (40) for $\theta_0 = \theta_{cr}$, fragmentation permits a significant increase in B_Σ and, hence, in the pulse compression factor with retention of the same G value. For $G = 1000$, e.g., dividing the nonlinear element into $N = 4$ parts permits increasing B_Σ by unity, into $N = 8$ parts by two, and into $N = 12$ parts by three.

It is possible to achieve an even stronger SSSF suppression by using nonlinear elements with significantly different values of n_2 in combination with intensity control in the elements (in this case, use should be made of a converging or diverging beam). Then, the peaks of noise gain $K_{av1,2}$ in two (or more) nonlinear elements are found at significantly different θ, which lowers the overall gain $K_{av1}K_{av2}$.

Lastly, accommodating nonlinear elements with different n_2 values immediately adjacent to each other (without an air gap) permits using both phase and amplitude effects. In this case, the transfer matrix U is the product of matrices (32). Modern technologies permit the fabrication of samples consisting of two films with different physical properties pressed to each other without a gap. A detailed consideration of the efficiency of SSSF suppression in a sequence of nonlinear elements with different n_2 values is the subject of a separate investigation.

The optical configurations in which SSSF suppression is realized by nonlinear element fragmentation are much more compact than those utilizing the self-filtering of a laser beam. At the same time, these two methods may be combined, for instance, as shown in Fig. 17 (image *4*). In this case, compactness is lost, but the noise suppression efficiency becomes higher. Fragmenting the nonlinear element, like two-stage compression, requires the use of very thin samples, which is easier to realize with plastic, especially so when $N \gg 1$. Therefore, polymers make it possible to improve the CafCA efficiency for a variety of reasons.

6. Compression after compressor approach (CafCA): status quo and prospects

The experimental data which demonstrate the energy parameters of input laser pulses in relation to the beam diameter, as well as the growth of pulse energy in the period of 1968–2018, are summarized in Fig. 3. As seen from the figure, several recent years have seen a remarkable CafCA advancement [22, 76–85] to the domain of high power (up to 250 TW) and energy (up to 15 J) owing to the use of a volume solid nonlinear element, in which the laser beam propagates freely. These data are marked with dots in Fig. 3. Below, we discuss the CafCA efficiency attained in these studies, the prospects of advancing to the multiterawatt range, and possible avenues of future investigations.

6.1 Review of experiments with a pulse power of 0.2–250 TW

From the practical viewpoint, one of the most important CafCA characteristics is the intensity enhancement factor F_i (10c). Direct measurements of the pulse intensity prior to and after compression are practically completely lacking, and so we will analyze the pulse compression factor F_τ (10b), which has been measured in all studies. Theoretically, F_τ is always smaller than F_i, but the difference is not large (compare Figs 4b and 4c). For a zero dispersion ($D = 0$, red points) the difference amounts to about 15%, while for a strong dispersion ($D = 0.05$, black points) the coefficients barely differ. To compare the magnitudes of F_i and F_τ, it is convenient to use formulas (11b, c) with the inclusion of Table 1. Therefore, parameter F_τ is easily measured and adequately reflects not only the pulse shortening but also the increase in pulse intensity.

The experimental data in Refs [22, 77–85] are summarized in Table 3. The values of F_τ as functions of the B-integral are shown with blue dots in Fig. 19. The straight lines were plotted for the theoretical dependences (11b) for $D = 0$ and $D = 0.05$. In many studies, for a nonlinear medium use was made of a plastic with unknown dispersion coefficient, and so there is no way of determining D. Nevertheless, it is highly likely that in all studies $D < 0.05$, i.e., that the experimental points in the plot should lie between the two straight lines. However, almost all points are lower. One of the reasons is the difference between the dispersion introduced by dispersive

Table 3. Experimental results from Refs [22, 77–85].

Input beam					Nonlinear element		*B*-integral	Pulse duration			References	Year
P, TW	W, mJ	d, mm	I, TW cm^{-2}	λ_0, nm	Material	L, mm		T_{in}, fs	T_{out}, fs	$F_\tau = T_{in}/T_{out}$		
0.6	28	5.2	0.94	800	TF12 (negative lens)	0.2	4.4	46	20	2.3	Mironov [77]	2014
5.2	170	38	0.84	800	TF12 (negative lens)	0.3	5.9	33	16	2.1	Lassonde [78]	2016
0.3	20	20	0.19	910	Polyethylene terephthalate	3	2.2	66	32	2.1	Ginzburg [83] Mironov [79]	2016 2017
4.3	200	11	1.4	810	Cellulose acetate	0.5	3.3	46	29	1.6	Mironov [79]	2017
96	5500	100	1.5	920	Polyethylene terephthalate	0.5	3.1	57	22	2.6	Mironov [80]	2017
5.4	296	19	1.9	810	Silica	0.5	2.2	55	31	1.8	Farinella [82]	2019
50	2400	99	0.65	810	Silica	0.5	0.8	48	42	1.1		
3.2	158	18	1.25	800	Zeonor	0.6	3.5	50	23	2.2	Masruri [81]	2019
1.5	75	18	0.59	800	Zeonor	0.6	1.7	50	33	1.5		
190	12,000	160	1.1	920	Glass	3	6	63	21	3	Ginzburg [22]	2019
250	16,000	160	1.3	910	Glass	3	7	65	15.5	4.1	Ginzburg [84, 85]	2019
250	17,000	160	1.0 *	910	Glass (two stages)	3 + 1.3	5.5 *	72	14.5	5		

* Values for the first stage.

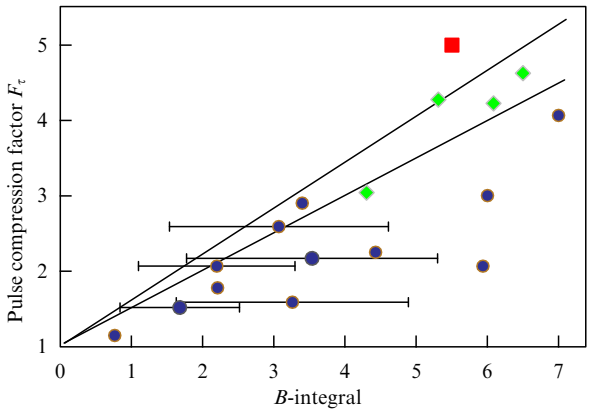

Figure 19. (Color online.) Pulse compression factor F_τ versus the *B*-integral. Blue dots show the experimental values obtained in Refs [22, 77–84] (see also Table 3), the red square corresponds to the two-stage CafCA of Ref. [85] (the *B* value corresponds to the *B*-integral of only the first stage), and diamonds stand for the numerical simulation data of Refs [20, 79, 87]. Straight lines were plotted for theoretical dependences (11) for zero dispersion $D = 0$ (upper straight line) and for $D = 0.05$ (lower straight line).

mirrors and the optimal value α_{opt}. Also possible are errors in the evaluation of the *B*-integral, especially so for experiments with the use of plastics. When plotting Fig. 19 for these data, we assumed the value of n_2 to be two times greater than for silica and indicated an error of 50% for the *B*-integral. The measurements of n_2 for different plastics is the subject of future investigations. In any case, a more than twofold pulse shortening was obtained in the majority of papers. A record fourfold shortening was obtained in Ref. [84] and for a record high input pulse power of 250 TW. In a first for high-power lasers, in Ref. [85] two CafCA stages were implemented and a fivefold duration shortening was demonstrated.

As stated in Section 3.2, for super-Gaussian transverse intensity distributions, transverse beam nonuniformity results in an insignificant lowering of CafCA efficiency: the increase in power is only slightly lower than that in intensity, $F_p < F_i$ (compare formulas (17) and (11c)). This issue has not been studied in experiments. At the same time, as applied to a laser beam with a Gaussian spatial intensity distribution, for which this effect is significant ($F_p = 0.5F_i$), its transverse nonuniformity was successfully compensated with a negative lens [77, 78] (see Section 3.2.2).

Another parasitic effect for CafCA is the nonlinear phase distortion introduced into a laser beam by cubic nonlinearity, which impairs the beam quality and lowers the focal intensity (see Section 3.3). Detailed experimental studies of this problem are also the subject of future investigations. We mention only Ref. [82], where an 11.4% lowering of the Strehl number was measured for $B = 0.8$; however, a quantitative comparison with formula (25) and with Fig. 12 is impossible, since the data about near-field beam shape were not reported in Ref. [82].

Figure 20 shows the experimental data in Refs [22, 77–85] in the plane (T_{in}, T_{out}) — the half-height durations of input and compressed pulses. As is clear from the figure, mastered to date is the range of several tens of femtoseconds for the duration of input pulses. We mention Ref. [78], in which a record short input pulse was obtained, and Ref. [85], in which it was possible to obtain (for a two-stage compression) the shortest pulse at the CafCA output. At the same time, so far there are no examples of successful experimental use of CafCA as applied to high-power (over 0.1 TW) laser pulses with a duration shorter than 30 fs or longer than 100 fs. The theoretical aspects for the specified parameters are discussed in Sections 2.3, 2.4, and 4.4. Here, we restrict ourselves to a brief outline of numerical simulation data.

6.2 Numerical CafCA simulations for petawatt pulses

Not many studies were devoted to numerical CafCA simulations for ultrahigh-power pulses [20, 79, 87]. The results are shown with diamonds in Figs 19 and 20. Investigated in

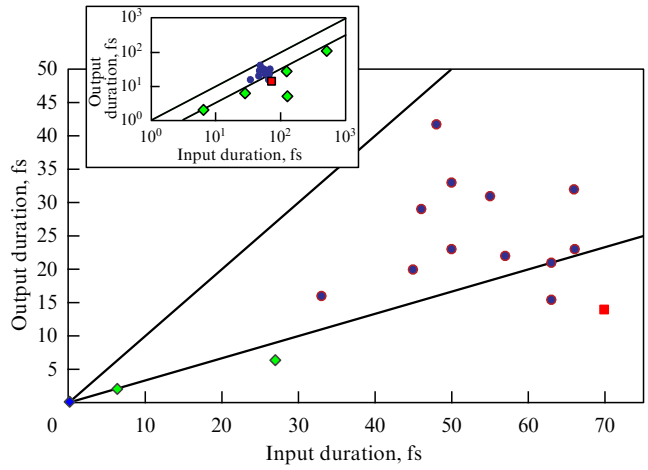

Figure 20. (Color online.) Experimental data from Refs [22, 77–84] (blue dots). Red square corresponds to the two-stage CafCA in Ref. [85] (see also Table 3) and diamonds stand for the numerical simulation data in Refs [20, 79, 87]. Straight lines show dependences $T_{\text{out}} = T_{\text{in}}$ and $T_{\text{out}} = T_{\text{in}}/3$ for clarity.

Ref. [20] was the two-stage compression of a single-petawatt 27-femtosecond-long pulse to 6.4 fs and then to 2.1 fs. In this case, simulations were made of Eqn (4) with all the terms with the exception of the Laplacian term, i.e., all temporal effects were included, but the self-focusing was not. It is significant that delivered to the input of the second CafCA stage was not a spectrally limited pulse, but the simulation result from the output of the first stage with compensation of only the quadratic component of the spectral phase. At the first stage $B = 6.1$, which implies suppression of SSSF, e.g., by self-filtering (see Section 4.3). At the second stage ($B = 4.4$), the SSSF was suppressed due to nonlinear dispersion, with account taken of the input pulse duration of 6.4 fs [109, 110] (see Section 4.4). We emphasize that the beam intensity at the input of the second stage was extremely high ($I = 43$ TW cm^{-2}). In practice, in order to avoid optical breakdown, it is necessary to increase the beam diameter and the nonlinear element thickness L with retention of the requisite B-integral value. Increasing the diameter will lower the intensity and, as a consequence, will rule out the breakdown probability. Increasing the thickness will strengthen the influence of linear dispersion on the pulse parameters at the output of the nonlinear element. For the CafCA efficiency to remain high, it is necessary to monitor the fulfillment of condition $D \ll 1$ for a given value of the B-integral.

The most detailed CafCA simulation was performed in Ref. [87], where account was taken not only of all the effects described by Eqn (4), but also of ionization nonlinearity and the loss and dispersion introduced by the laser field-ionized plasma. Radiation of a 120-fs-long Gaussian pulse with a power of 13 PW and a beam diameter of 40 cm with a super-Gaussian intensity distribution ($m = 8$, $I = 11$ TW cm^{-2}) was delivered to the input of a nonlinear medium (fused quartz). To model SSSF, intensity modulation with an rms deviation of 0.1185 was introduced into the input beam. This modulation is equivalent to the amplitude noise (noise phase $\varphi_{\text{in}} = 0$ for all spatial frequencies), although random φ_{in} values correspond to the majority of experimental situations. According to formula (41), for an rms deviation of 0.0185, the noise power fraction amounts to 8.5×10^{-5}, which is greater than the value of 1.8×10^{-5} given in Ref. [175] for the power fraction scattered by high-precision optics into an angular spectrum band of 0.01–0.1 rad.

The results of simulations [87] suggest that the maximum admissible value of the B-integral is 5.3. In this case, the pulse compresses to 25 fs for a complete compensation of dispersion. In the compensation of only the quadratic spectral phase component, the duration will be somewhat longer (the simulation data indicated with different symbols in Figs 19 and 20 correspond to a duration of 28 fs). Another simulation result of Ref. [87] shown in the inset of Fig. 20 displays the simulation of CafCA in nine such quartz plates ($B_\Sigma = 48$) separated by eight spatial filters, which seems hardly realizable in practice. As shown in Section 5.3, the use of two-stage compression shows greater promise. We note that the simulations even for these extreme B-integral values showed very good beam focusing.

Investigated in Ref. [79] was the CafCA for a very long (500 fs) pulse using the example of a PETAL laser [124, 125] (transverse beam size: 40 cm; central wavelength: 1053 nm; energy: 1 kJ) under the assumption of transversely uniform intensity with $B = 6.5$ for a quartz plate of thickness $L = 3$ mm. The results of simulations confirmed a negligible effect of dispersion and showed that correcting the quadratic phase component of the output radiation permitted shortening the pulse duration to 108 fs and increasing the peak intensity from 1.5 TW cm^{-2} to 6 TW cm^{-2}. In this case, $\alpha_{\text{opt}} = -10^4$ fs^2, which agrees with Fig. 5b. Such a large value of parameter α_{opt} calls for an improvement in dispersive mirror fabrication technology and/or for a large number of these mirrors. We note that increasing B results in a lowering (in modulus) of α_{opt} (see Fig. 5). Thus, e.g., increasing B from 6.5 to 20 decreases α_{opt} by a factor of three.

6.3 Future research avenues

From the practical standpoint, the main task facing experimenters now is applying CafCA at the output of petawatt and multipetawatt lasers, especially with short (less than 30 fs) and long (longer than 100 fs) pulses. This will open the way to the development of next-generation pulses — several tens and hundreds of PW in power — as well as to the production of multipetawatt laser pulses with a duration of the order of one field cycle. The theoretical and experimental investigations described in our review suggest that there are no fundamental limitations on this route, although the problems are many. We list several lines of research that are topical for successful advancement along this route.

(1) Experimental measurements of precisely the focal-plane intensity enhancement factor F_{focus} rather than the pulse compression factor F_τ. These factors are different, because part of the pulse energy is away from the principal peak, with the result that the intensity after CafCA increases with a lower efficiency ($F_{\text{i}} < F_\tau$), and because the B-integral is nonuniformly distributed over the beam cross section, with the result that the power increases with a lower efficiency ($F_{\text{p}} < F_{\text{i}}$). Lastly, $F_{\text{focus}} < F_{\text{p}}$ due to nonlinear wavefront aberrations, which may be compensated using adaptive optics, if need be. These effects are theoretically discussed in detail in Sections 2.2, 3.3, and 3.2.1, where it is shown what can be achieved owing to an insignificant difference between F_{focus} and F_τ. However, to date, experimental confirmations have not been obtained.

(2) SSSF suppression for large B-integral values for increasing the pulse compression factor F_τ with one CafCA stage. Despite the substantial progress in this area, which

permitted the values $B = 7$ and $F_\tau = 4$ to be reached in experiments, further advancement is possible. Seeming most important are: (i) theoretical and experimental investigations of the spatial noise spectrum (see Section 4.2) in real ultrahigh-power laser beams, as well as optimization of the self-filtering of these beams (see Section 4.3) reliant on the resultant data and work to increase the critical angle (see Section 5.2); (ii) experimental realization of SSSF suppression due to nonlinear dispersion (see Section 4.4), the use of spatial filters (see Section 4.5.1), and the use of media with negative n_2 (see Section 4.5.2); (iii) theoretical and experimental investigations of the capabilities of the fragmentation of a nonlinear element (particularly a plastic one) for SSSF suppression (see Section 5.4).

(3) Experimental realization of a 10-fold (and greater) pulse compression, which is supposedly possible with a two-stage CafCA. Demonstrated recently was the two-stage compression of 250-TW pulses [85], and the results turned out to be promising, but a comprehensive experimental investigation is still to be done. The most attractive goals are the production of pulses with durations of the order of one optical field cycle and the compression of kilojoule-level pulses to a duration of the order of 10 fs.

(4) Measurement of the nonlinear refractive index n_2, group velocity dispersion k_2, and other optical properties of polymer materials (plastics). At present, these data barely exist in the literature. A wide variety of plastics gives hope for a diversity of their properties. This, in turn, will permit the optimal use of plastics to increase the compression multiplicity (see Section 5).

(5) Pulse compression for a simultaneous second harmonic generation. The phase self-modulation of pulses required for CafCA occurs automatically in any medium, including crystals generating a second harmonic. Owing to this circumstance, the second harmonic pulse may be compressed with dispersive mirrors. The idea was introduced in Ref. [73], the broadening of the second harmonic spectrum due to phase self-modulation was measured in Ref. [76], and the compression of second harmonic pulses was demonstrated in Ref. [232], though for pulses only 50 GW in power. The execution of similar experiments at a level of several hundred TW is limited by the difficulty of making nonlinear crystals, but these limitations may be overcome. This will permit increasing the focal intensity not only due to pulse compression, as with ordinary CafCA, but also due to wavelength shortening. Furthermore, the time contrast ratio of pulses will greatly increase, which is important for many applications.

7. Conclusions

The peak power of modern lasers is limited by the breakdown threshold of the diffraction gratings of optical compressors. Pulse compression after a compressor (CafCA) is one of the most promising ways of overcoming this barrier, because the power of a pulse increases due to its shortening rather than due to its energy increase. The pulse spectrum broadens due to phase self-modulation in the medium with a Kerr nonlinearity, and then the pulse is compressed on reflection from dispersive mirrors. CafCA possesses indubitable merits: simplicity and cheapness, negligible energy loss, and the possibility of using it in any high-power laser. The main conclusions may be formulated as follows.

(1) In the one-dimensional quasistationary approximation, pulse shortening is determined by nonlinearity and dispersion, which are quantitatively characterized by the B-integral (3) and parameter D (7). In ultrahigh-power lasers, use is made, as a rule, of very thin nonlinear elements ($D < 0.05$), and dispersion plays a minor role. In this case, the pulse intensity increase to a value $B = 13$ is nicely described by the formula $I_{out}/I_{in} = 1 + 0.49B$. The role of dispersion comes down to an insignificant lowering of the effective value of B (11). When the input pulse is not spectrally limited, the I_{out}/I_{in} ratio does not change significantly (see Fig. 9). When dispersive mirrors not only introduce a quadratic spectral phase but also provide a Fourier-limited pulse at the CafCA output, I_{out} increases by about 10%.

(2) The spatial beam nonuniformity (especially for large B) results in a lowering of focal intensity due to nonlinear wavefront distortions and the lowering of the compression factor at the beam periphery. The cross section-averaged compression factor for a super-Gaussian beam of order $m \geqslant 4$ is lower by no more than 8% than the compression factor for a flat-top beam. For close-to-Gaussian beams, it is necessary to employ a nonlinear element in the form of a negative lens (see Section 3.2.2) and correct the phase aberrations with an adaptive mirror.

(3) The main limitation on the use of CafCA in high-power lasers is small-scale self-focusing. A fundamentally important special feature of SSSF in ultrahigh-power femtosecond lasers in comparison with that in nanosecond lasers is a significant increase in SSSF critical angle θ_{cr} (30) — up to several tens of milliradians. This results in relaxation of the heretofore inviolable limitation $B < 2-3$, whereby the power may be increased by only 2–2.5 times. Furthermore, large θ_{cr} values permit using beam self-filtering in the free-space propagation for SSSF suppression: the most 'dangerous' noise components (with θ of the order of θ_{max}) escape from the beam aperture (see Section 4.3). For few-cycle laser pulses (i.e., for pulses 25 fs or less in duration), an additional mechanism of SSSF suppression appears: nonlinear dispersion — the intensity dependence of the group velocity (see Section 4.4). Therefore, SSSF suppression by these and other methods makes it possible to significantly increase the admissible B-integral values and, accordingly, increase the multiplicity of compression. To date, the efficiency of CafCA has been experimentally demonstrated for $B = 7$ (see Fig. 19).

(4) The use of polymer materials (plastics) as nonlinear elements substantially extends the capabilities of CafCA. Plastics offer a number of advantages: a practically unlimited aperture, a thickness of 100 μm and even less, manufacturability, low cost, and a wide variety of materials, which gives hope for a diversity of properties, as well as the possibility of SSSF suppression due to nonlinear element fragmentation (replacement of one element by several elements with the same total B-integral) and due to increasing the critical angle θ_{cr}. In particular, a 2.6-fold compression of a 100-TW-power pulse was obtained with the use of a plastic.

(5) An important advantage of CafCA is the possibility of two-stage (or even multistage) compression (see Fig. 17), since the total power enhancement factor depends on the number of stages according to a power law (51), while the total B-integral B_Σ, which determines all parasitic effects, depends linearly on the number of stages. For $B_\Sigma > 5$, the increase in the number of stages to two and, even more so, to three makes it possible to obtain a significantly higher power of the compressed pulse. Furthermore, it is easier to suppress SSSF with a two-stage compression (see Section 5.3). Recent experiments have demonstrated a five-fold pulse compres-

sion in the two-stage CafCA, but the potentialities are much wider.

(6) The experimental results of using CafCA are presented in Figs 19 and 20 (see also Fig. 3 and Table 3). A range of input pulse parameters from several TW in power up to 15 J in energy and from 30 to 80 fs in duration has been mastered to date. A fourfold pulse compression has been demonstrated with one stage and a fivefold one with two stages. Within the next few years, one would expect the wide use of CafCA, including the two-stage one, in petawatt and multipetawatt lasers, in particular with 15–25-fs-long pulses, as well as in kilojoule lasers with a pulse duration of several hundred femtoseconds. Furthermore, a higher pulse compression multiplicity (by several dozen times) will be achieved and direct measurements will be made of a multiple increase in the focal-plane intensity.

Acknowledgements

The authors express their gratitude to V N Ginzburg, A A Kochetkov, A K Potemkin, A M Sergeev, I V Yakovlev, and J Wheeler for helpful discussions.

This work was supported by the Ministry of Science and Higher Education of the Russian Federation in the framework of the Federal Dedicated Program "Investigation and Development in Priority Development Lines of the Scientific-Technological Complex of Russia in 2014-2020" (grant no. 14.607.21.0196; unique identification number of the project: RFMEFI60717X0196).

References

1. Maiman T H *Nature* **187** 493 (1960)
2. Mourou G A, Barty C P J, Perry M D *Phys. Today* **51** (1) 22 (1998)
3. Strickland D, Mourou G *Opt. Commun.* **56** 219 (1985)
4. Abbott B P et al. (LIGO Scientific Collab., Virgo Collab.) *Phys. Rev. Lett.* **116** 061102 (2016)
5. Treacy E B *Phys. Lett. A* **28** 34 (1968)
6. Treacy E *IEEE J. Quantum Electron.* **5** 454 (1969)
7. Martinez O *IEEE J. Quantum Electron.* **23** 59 (1987)
8. Pessot M, Maine P, Mourou G *Opt. Commun.* **62** 419 (1987)
9. Offner A, US Patent 3,748,015 (1971)
10. Yakovlev I V *Quantum Electron.* **44** 393 (2014); *Kvantovaya Elektron.* **44** 393 (2014)
11. Bahk S-W et al. *Appl. Phys. B* **80** 823 (2005)
12. Bahk S-W et al. *Opt. Lett.* **29** 2837 (2004)
13. *LLE Rev. Quart. Rep.* **115** (2008)
14. Hornung M et al. *Appl. Opt.* **46** 7432 (2007)
15. Cotel A et al. *Opt. Express* **15** 2742 (2007)
16. Blanchot N et al. *Opt. Express* **25** 16957 (2017)
17. Blanchot N et al. *Opt. Express* **18** 10088 (2010)
18. Shaykin A et al. *Rev. Laser Eng.* **42** 141 (2014)
19. Frolov S A et al. *Quantum Electron.* **48** 335 (2018); *Kvantovaya Elektron.* **48** 335 (2018)
20. Mourou G et al. *Eur. Phys. J. Spec. Top.* **223** 1181 (2014)
21. Danson C et al. *High Power Laser Sci. Eng.* **7** e54 (2019)
22. Ginzburg V N et al. *Quantum Electron.* **49** 299 (2019); *Kvantovaya Elektron.* **49** 299 (2019)
23. Pervak V et al. *Opt. Express* **16** 10220 (2008)
24. Steinmeyer G *Appl. Opt.* **45** 1484 (2006)
25. Szipöcs R et al. *Opt. Lett.* **19** 201 (1994)
26. Pervak V et al. *Appl. Phys. B* **87** 5 (2007)
27. Matuschek N et al. *Appl. Phys. B* **71** 509 (2000)
28. Giordmaine J, Duguay M, Hansen J *IEEE J. Quantum Electron.* **4** 252 (1968)
29. Klauder J R *Bell Syst. Tech. J.* **39** 809 (1960)
30. Klauder J R et al. *Bell Syst. Tech. J.* **39** 745 (1960)
31. Duguay M A, Hansen J W *Appl. Phys. Lett.* **14** 14 (1969)
32. Gires F, Tournois P *C.R. Acad. Sci. Paris* **258** 6112 (1964)
33. Fisher R A, Kelley P L, Gustafson T K *Appl. Phys. Lett.* **14** 140 (1969)
34. Laubereau A *Phys. Lett. A* **29** 539 (1969)
35. Lehmberg R H, McMahon J M *Appl. Phys. Lett.* **28** 204 (1976)
36. Zhou J Y et al. *Opt. Lett.* **16** 1865 (1991)
37. Nakatsuka H, Grischkowsky D, Balant A C *Phys. Rev. Lett.* **47** 910 (1981)
38. Shank C V et al. *Appl. Phys. Lett.* **40** 761 (1982)
39. Grischkowsky D, Balant A C *Appl. Phys. Lett.* **41** 1 (1982)
40. Tomlinson W J, Stolen R H, Shank C V *J. Opt. Soc. Am. B* **1** 139 (1984)
41. Meinel R *Opt. Commun.* **47** 343 (1983)
42. Fujimoto J G, Weiner A M, Ippen E P *Appl. Phys. Lett.* **44** 832 (1984)
43. Nikolaus B, Grischkowsky D *Appl. Phys. Lett.* **43** 228 (1983)
44. Knox W H et al. *Appl. Phys. Lett.* **46** 1120 (1985)
45. Nikolaus B, Grischkowsky D *Appl. Phys. Lett.* **42** 1 (1983)
46. Halbout J-M, Grischkowsky D *Appl. Phys. Lett.* **45** 1281 (1984)
47. Fork R L et al. *Opt. Lett.* **12** 483 (1987)
48. Damm T et al. *Opt. Lett.* **10** 176 (1985)
49. Lin K-C, Lin Y-C *Opt. Laser Technol.* **44** 1733 (2012)
50. Limpert J et al. *Appl. Phys. B* **74** 191 (2002)
51. Calvani R, Caponi R, Grazioli E *Fiber Integrat. Opt.* **17** 41 (1998)
52. Yamashita M, Torizuka K *Jpn. J. Appl. Phys.* **29** 294 (1990)
53. Lefort C et al. *Opt. Lett.* **36** 292 (2011)
54. Seidel M, Xiao X, Hartung A *IEEE J. Select. Top. Quantum Electron.* **24** 510098 (2018)
55. Klenke A et al. *Opt. Lett.* **39** 3520 (2014)
56. Nisoli M, De Silvestri S, Svelto O *Appl. Phys. Lett.* **68** 2793 (1996)
57. Moulton P F *J. Opt. Soc. Am. B* **3** 125 (1986)
58. Schenkel B et al. *Opt. Lett.* **28** 1987 (2003)
59. Hort O et al. *J. Opt. Soc. Am. B* **32** 1055 (2015)
60. Cardin V et al. *Appl. Phys. Lett.* **107** 181101 (2015)
61. Chen X et al. *Opt. Lett.* **34** 1588 (2009)
62. Akturk S et al. *Opt. Lett.* **34** 1462 (2009)
63. Suda A et al. *Appl. Phys. Lett.* **86** 111116 (2005)
64. Jeong Y-G et al. *Sci. Rep.* **8** 11794 (2018)
65. Petrov V, Rudolph W, Wilhelmi B *J. Mod. Opt.* **36** 587 (1989)
66. Rolland C, Corkum P B *J. Opt. Soc. Am. B* **5** 641 (1988)
67. Mével E et al. *J. Opt. Soc. Am. B* **20** 105 (2003)
68. Reitze D H, Weiner A M, Leaird D E *Opt. Lett.* **16** 1409 (1991)
69. Seidel M et al. *Opt. Express* **24** 9412 (2016)
70. He P et al. *Opt. Lett.* **42** 474 (2017)
71. Schulte J et al. *Opt. Lett.* **41** 4511 (2016)
72. Mak A A, Yashin V E *Opt. Spectrosc.* **70** 1 (1991); *Opt. Spektrosk.* **70** 3 (1991)
73. Mironov S et al. *Appl. Opt.* **48** 2051 (2009)
74. Mourou G, US Patent 20110299152 A1 (2009)
75. Mourou G F et al. Frances Patent FR3017495 (B1) (2014)
76. Mironov S Yu et al. *Quantum Electron.* **41** 963 (2011); *Kvantovaya Elektron.* **41** 963 (2011)
77. Mironov S et al. *Eur. Phys. J. Spec. Top.* **223** 1175 (2014)
78. Lassonde P et al. *Laser Phys. Lett.* **13** 075401 (2016)
79. Mironov S Yu et al. *Quantum Electron.* **47** 173 (2017); *Kvantovaya Elektron.* **47** 173 (2017)
80. Mironov S Yu et al. *Quantum Electron.* **47** 614 (2017); *Kvantovaya Elektron.* **47** 614 (2017)
81. Masruri M et al., in *Proc. SPIE* (2019) in press
82. Farinella D M et al. *J. Opt. Soc. Am. B* **36** A28 (2019)
83. Ginzburg V N et al. *Quantum Electron.* **46** 106 (2016); *Kvantovaya Elektron.* **46** 106 (2016)
84. Ginzburg V N et al., in *Proc. of the 8th Intern. Conf.* "*Frontiers of Nonlinear Physics*", *Nizhny Novgorod, Russia, June 28 – July 4, 2019*
85. Ginzburg V N et al. *Phys. Rev. A* (2019) to be published
86. Mironov S Yu et al. *IEEE J. Select. Top. Quantum Electron.* **18** 7 (2010)
87. Voronin A A et al. *Opt. Commun.* **291** 299 (2013)
88. Andreev A A et al. *Quantum Electron.* **27** 95 (1997); *Kvantovaya Elektron.* **24** 99 (1997)
89. Mironov S Yu et al. *Quantum Electron.* **43** 711 (2013); *Kvantovaya Elektron.* **43** 711 (2013)

90. Bespalov V I, Talanov V I *JETP Lett*. **3** 307 (1966); *Pis'ma Zh. Eksp. Teor. Fiz*. **3** 471 (1966)
91. Mak A A et al. *Lazery na Neodimovom Stekle* (Neodymium Glass Lasers) (Ed. A A Mak) (Moscow: Nauka, 1990)
92. Bondarenko N G et al. *JETP Lett*. **12** 85 (1970); *Pis'ma Zh. Eksp. Teor. Fiz*. **12** 125 (1970)
93. Vlasov S N, Koposova E V, Yashin V E *Quantum Electron*. **42** 989 (2012); *Kvantovaya Elektron*. **42** 989 (2012)
94. Mironov S Yu et al. *Laser Phys. Lett*. **12** 025301 (2015)
95. Shimizu F *Phys. Rev. Lett*. **19** 1097 (1967)
96. Gustafson T K et al. *Phys. Rev*. **177** 306 (1969)
97. Alfano R R, Shapiro S L *Phys. Rev. Lett*. **24** 592 (1970)
98. Fisher R A, Bischel W K *J. Appl. Phys*. **46** 4921 (1975)
99. Fisher R A, Bischel W *Appl. Phys. Lett*. **23** 661 (1973)
100. Ostrovskii L A *Sov. Phys. Tech. Phys*. **8** 679 (1964); *Zh. Tekh. Fiz*. **33** 905 (1963)
101. Ostrovskii L A *Sov. Phys. JETP* **24** 797 (1967); *Zh. Eksp. Teor. Fiz*. **51** 1189 (1966)
102. Litvak A G, Talanov V I *Izv. Vyssh. Uchebn. Zaved. Radiofiz*. **10** 539 (1967)
103. Kandidov V P et al. *Quantum Electron*. **34** 348 (2004); *Kvantovaya Elektron*. **34** 348 (2004)
104. Zharova N A, Litvak A G, Mironov V A *Radiophys. Quantum Electron*. **46** 297 (2003); *Izv. Vyssh. Uchebn. Zaved. Radiofiz*. **46** 331 (2003)
105. Gromov E M, Talanov V I *Radiophys. Quantum Electron*. **41** 143 (1998); *Izv. Vyssh. Uchebn. Zaved. Radiofiz*. **41** 222 (1998)
106. Zakharov V E, Kuznetsov E A *Phys. Usp*. **40** 1087 (1997); *Usp. Fiz. Nauk* **167** 1137 (1997)
107. Anderson D, Lisak M *Phys. Rev. A* **27** 1393 (1983)
108. Zheltikov A *Opt. Express* **26** 17571 (2018)
109. Balakin A A et al. *J. Opt*. **19** 095503 (2017)
110. Balakin A A et al. *Phys. Rev*. **94** 043812 (2016)
111. Grudtsyn Ya V et al. *Quantum Electron*. **49** 302 (2019); *Kvantovaya Elektron*. **49** 302 (2019)
112. Grudtsyn Ya V et al. *Quantum Electron*. **48** 306 (2018); *Kvantovaya Elektron*. **48** 306 (2018)
113. Akhmanov S A, Vysloukh V A, Chirkin A S *Optics of Femtosecond Laser Pulses* (New York: American Institute of Physics, 1992); Translated from Russian: *Optika Femtosekundnykh Lazernykh Impul'sov* (Moscow: Nauka, 1988)
114. Shumakova V et al. *Nature Commun*. **7** 12877 (2016)
115. Voronin A A, Zheltikov A M *Phys. Rev. A* **94** 023824 (2016)
116. Hemmer M et al. *Opt. Express* **21** 28095 (2013)
117. Voronin A A, Zheltikov A M *Phys. Usp*. **69** 869 (2016); *Usp. Fiz. Nauk* **186** 957 (2016)
118. Schmidt B E et al. *Appl. Phys. Lett*. **96** 121109 (2010)
119. Bergé L, Mauger S, Skupin S *Phys. Rev. A* **81** 013817 (2010)
120. Brabec T, Krausz F *Phys. Rev. Lett*. **78** 3282 (1997)
121. Gustafson T K et al. *Phys. Rev*. **177** 306 (1969)
122. DeMartini F et al. *Phys. Rev*. **164** 312 (1967)
123. Gaul E W et al. *Appl. Opt*. **49** 1676 (2010)
124. Batani D et al. *Phys. Scripta* **2014** 014016 (2014)
125. Blanchot N et al. *Plasma Phys. Control. Fusion* **50** 124045 (2008)
126. Bagnoud V et al. *Appl. Phys. B* **100** 137 (2010)
127. Lozhkarev V V et al. *Laser Phys. Lett*. **4** 421 (2007)
128. Chekhlov O V et al. *Opt. Lett*. **31** 3665 (2006)
129. Ren Z et al. *High Power Laser Sci. Eng*. **6** 1 (2018)
130. Skobelev S A, Kartashov D V, Kim A V *Phys. Rev. Lett*. **99** 203902 (2007)
131. Leblond H, Mihalache D *Phys. Rep*. **523** 61 (2013)
132. Kim A V, Skobelev S A *Phys. Rev. A* **83** 063832 (2011)
133. Bespalov V G et al. *Phys. Rev. A* **66** 013811 (2002)
134. Gol'dberg V N, Talanov V I, Erm R E *Radiophys. Quantum Electron*. **14** 368 (1967); *Izv. Vyssh. Uchebn. Zaved. Radiofiz*. **10** 674 (1967)
135. Kelley P L *Phys. Rev. Lett*. **15** 1005 (1965)
136. Mironov S Y et al., US Patent US9678405 (2014)
137. Hunt J T, Renard P A, Nelson R G *Appl. Opt*. **15** 1458 (1976)
138. Siegman A E *Proc. SPIE* **1224** 2 (1990)
139. Strehl K *Z. Instrumentenkd* **22** 213 (1902)
140. Potemkin A K, Khazanov E A *Quantum Electron*. **35** 1042 (2005); *Kvantovaya Elektron*. **35** 1042 (2005)
141. Vlasov S N, Petrishchev V A, Talanov V I *Radiophys. Quantum Electron*. **14** 1062 (1974); *Izv. Vyssh. Uchebn. Zaved. Radiofiz*. **14** 1353 (1971)
142. Perevezentsev E, Poteomkin A, Khazanov E *Appl. Opt*. **46** 774 (2007)
143. Parent A, Morin M, Lavigne P *Opt. Quantum Electron*. **24** S1071 (1992)
144. Wang H et al. *Opt. Express* **27** 404 (2019)
145. Alaluf D et al. *Appl. Opt*. **57** 3629 (2018)
146. Abbi S C, Kothari N C *J. Appl. Phys*. **51** 1385 (1980)
147. Fleck J A, Morris J, Bliss E *IEEE J. Quantum Electron*. **14** 353 (1978)
148. Suydam B R *IEEE J. Quantum Electron*. **11** 225 (1975)
149. Jokipii J R, Marburger J *Appl. Phys. Lett*. **23** 696 (1973)
150. Brueckner K A, Jorna S *Phys. Rev. Lett*. **17** 78 (1966)
151. Vlasov S N, Yashin V E *Sov. J. Quantum Electron*. **11** 510 (1981); *Kvantovaya Elektron*. **8** 510 (1981)
152. Vlasov S N *Sov. J. Quantum Electron*. **6** 245 (1981); *Kvantovaya Elektron*. **3** 451 (1976)
153. Vlasov S N *Sov. Phys. Tech. Phys. Lett*. **4** 320 (1978); *Pis'ma Zh. Tekh. Fiz*. **4** 795 (1978)
154. Rozanov N N, Smirnov V A *Sov. Phys. Tech. Phys. Lett*. **5** 222 (1979); *Pis'ma Zh. Tekh. Fiz*. **5** 544 (1979)
155. Vlasov S N, Yashin V E *Sov. J. Quantum Electron*. **10** 232 (1980); *Kvantovaya Elektron*. **7** 410 (1980)
156. Suydam B R *IEEE J. Quantum Electron*. **10** 837 (1974)
157. Marburger J H *Prog. Quantum Electron*. **4** 35 (1975)
158. Carman R L, Chiao R Y, Kelley P L *Phys. Rev. Lett*. **17** 1281 (1966)
159. Chiao R Y, Kelley P L, Garmire E *Phys. Rev. Lett*. **17** 1158 (1966)
160. Chilingaryan Yu S *Sov. Phys. JETP* **28** 1200 (1969); *Zh. Eksp. Teor. Fiz*. **55** 1589 (1968)
161. Bliss E S et al. *Appl. Phys. Lett*. **25** 448 (1974)
162. Campillo A J, Shapiro S L, Suydam B R *Appl. Phys. Lett*. **24** 178 (1974)
163. Campillo A J, Shapiro S L, Suydam B R *Appl. Phys. Lett*. **23** 628 (1973)
164. Abbi S C, Mahr H *Appl. Phys. Lett*. **19** 415 (1971)
165. Ginzburg V N et al. *Quantum Electron*. **47** 248 (2017); *Kvantovaya Elektron*. **47** 248 (2017)
166. Ginzburg V N et al. *Quantum Electron*. **40** 503 (2010); *Kvantovaya Elektron*. **40** 503 (2010)
167. Kuz'mina M S, Khazanov E A *Radiophys. Quantum Electron*. **59** 596 (2016); *Izv. Vyssh. Uchebn. Zaved. Radiofiz*. **59** 660 (2016)
168. Kuz'mina M S, Khazanov E A *Quantum Electron*. **43** 21 (2013); *Kvantovaya Elektron*. **43** 21 (2013)
169. Ginzburg V N et al. *Quantum Electron*. **48** 325 (2018); *Kvantovaya Elektron*. **48** 325 (2018)
170. Grow T D, Gaeta A L *Opt. Express* **13** 4594 (2005)
171. Boyd R W, Lukishova S G, Shen Y R (Eds) *Self-focusing*: *Past and Present. Fundamentals and Prospects* (Topics in Appl. Phys., Vol. 114) (New York: Springer, 2009) https://doi.org/10.1007/978-0-387-34727-1
172. Liu R et al. *Opt. Express* **24** 2293 (2016)
173. Garanin S G et al. *Quantum Electron*. **37** 1159 (2007); *Kvantovaya Elektron*. **37** 1159 (2007)
174. Poteomkin A K et al. *IEEE J. Quantum Electron*. **45** 336 (2009)
175. Spaeth M L et al. *Opt. Eng*. **43** 2854 (2004)
176. Campbell J H et al. *Proc. SPIE* (2004)
177. Ginzburg V N et al. *Radiophys. Quantum Electron*. (2019) to be published; *Izv. Vyssh. Uchebn. Zaved. Radiofiz*. (2019) to be published
178. Xiao-Fang L et al. *Chinese Phys. Lett*. **23** 3278 (2006)
179. Mironov S et al. *Appl. Phys. B* **113** 147 (2013)
180. Kochetkova M S et al. *Quantum Electron*. **39** 923 (2009); *Kvantovaya Elektron*. **39** 923 (2009)
181. Weber M J et al. *Opt. Commun*. **18** 171 (1975)
182. Vlasov S N, Talanov V I *Samofokusirovka Voln* (Wave Self-Focusing) (Nizhny Novgorod: Institut Prikladnoi Fiziki RAN, 1997)
183. Poteomkin A K et al. *IEEE J. Quantum Electron*. **45** 854 (2009)

184. Khazanov E A et al. *Opt. Express* **25** 27968 (2017)
185. Jain M et al. *Phys. Rev. Lett.* **75** 4385 (1995)
186. Baranova N B et al. *Tr. Fiz. Inst. Akad. Nauk SSSR* **103** 84 (1978)
187. Basov N G et al. *Sov. J. Quantum Electron.* **9** 205 (1972); *Kvantovaya Elektron.* **6** 46 (1972)
188. Kryukov P G et al. *Sov. J. Quantum Electron.* **3** 161 (1973); *Kvantovaya Elektron.* **2** 102 (1973)
189. Alexandrova I V et al. *Laser Part. Beams* **1** 241 (1983)
190. Mak A A et al. *Pis'ma Zh. Tekh. Fiz.* **6** 129 (1980)
191. Fedotov S I et al. *J. Russ. Laser Res.* **25** 79 (2004)
192. Maillotte H et al. *Opt. Commun.* **109** 265 (1994)
193. Maillotte H, Monneret J, Froehly C *Opt. Commun.* **77** 241 (1990)
194. Vysotina N V, Rosanov N N, Yashin V E *Opt. Spectrosc.* **110** 973 (2011); *Opt. Spektrosk.* **110** 1029 (2011)
195. Hunt J T, Renard P A, Simmons W W *Appl. Opt.* **16** 779 (1977)
196. Simmons W W, Speck D, Hunt J *IEEE J. Quantum Electron.* **13** 862 (1977)
197. Simmons W et al. *IEEE J. Quantum Electron.* **11** 852 (1975)
198. Alekseev V N et al. *Sov. J. Quantum Electron.* **9** 981 (1979); *Kvantovaya Elektron.* **6** 1666 (1979)
199. Bayanov V I et al. *Sov. J. Quantum Electron.* **9** 535 (1979); *Kvantovaya Elektron.* **6** 902 (1979)
200. Bunkenberg J et al. *IEEE J. Quantum Electron.* **17** 1620 (1981)
201. Garanin S G et al. *Quantum Electron.* **35** 299 (2005); *Kvantovaya Elektron.* **35** 299 (2005)
202. Hunt J T et al. *Appl. Opt.* **17** 2053 (1978)
203. Kuz'mina N V et al. *Opt. Spektrosk.* **51** 509 (1981)
204. Poteomkin A K et al. *Appl. Opt.* **46** 4423 (2007)
205. Potemkin A K et al. *Quantum Electron.* **35** 302 (2005); *Kvantovaya Elektron.* **35** 302 (2005)
206. Lehmberg R H, Reintjes J, Eckardt R C *Appl. Phys. Lett.* **25** 374 (1974)
207. Lehmberg R H et al. *Opt. Commun.* **121** 78 (1995)
208. Konoplev O A, Meyerhofer D D *IEEE J. Select. Top. Quantum Electron.* **4** 459 (1998)
209. Zhou X Q et al. *Appl. Phys. Lett.* **61** 3020 (1992)
210. Sheik-Bahae M et al. *IEEE J. Quantum Electron.* **27** 1296 (1991)
211. Meyerhofer D D, Konoplev O A, Grant US-6141362-A (1998)
212. Bache M et al. *Opt. Mater. Express* **3** 357 (2013)
213. Anis M et al. *Physica B* **449** 61 (2014)
214. Anis M, Hakeem D A, Muley G G *Results Phys.* **6** 645 (2016)
215. Baig M I, Anis M, Muley G G *Opt. Mater.* **72** 1 (2017)
216. Wang D et al. *RSC Adv.* **6** 14490 (2016)
217. Wang D et al. *Opt. Mater. Express* **7** 533 (2017)
218. Ostrovskii L A *JETP Lett.* **5** 272 (1967); *Pis'ma Zh. Eksp. Teor. Fiz.* **5** 331 (1967)
219. Stegeman G I, Hagan D J, Torner L *Opt. Quantum Electron.* **28** 1691 (1996)
220. DeSalvo R et al. *Opt. Lett.* **17** 28 (1992)
221. Ironside C N et al. *IEEE J. Quantum Electron.* **29** 2650 (1993)
222. Saltiel S, Koynov K, Buchvarov I *Appl. Phys. B* **63** 371 (1996)
223. Beckwitt K et al. *Opt. Lett.* **26** 1696 (2001)
224. Caumes J P et al. *Opt. Lett.* **29** 899 (2004)
225. Dorrer C et al. *Opt. Lett.* **39** 4466 (2014)
226. Seidel M et al. *Sci. Rep.* **7** 1410 (2017)
227. Liu X, Qian L, Wise F *Opt. Lett.* **24** 1777 (1999)
228. Zhou B B et al. *Phys. Rev. Lett.* **109** 043902 (2012)
229. Bykovskii N E et al. *Tr. Fiz. Inst. Akad. Nauk SSSR* **149** 150 (1985)
230. Baranova N B et al. *Sov. J. Quantum Electron.* **4** 1362 (1974); *Kvantovaya Elektron.* **1** 2450 (1974)
231. Baranova N B, Bykovskii N E, Senatskii Yu V *Sov. J. Quantum Electron.* **12** 105 (1982); *Kvantovaya Elektron.* **9** 161 (1982)
232. Alekseev S V et al. *Quantum Electron.* **49** 901 (2019); *Kvantovaya Elektron.* **49** 901 (2019)
233. Pinault S C, Potasek M J *J. Opt. Soc. Am. B* **2** 1318 (1985)